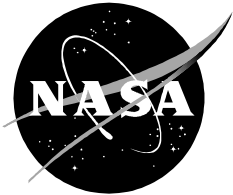NASA/TP—2000–209760

Oxidation of Reinforced Carbon-Carbon Subjected to Hypervelocity Impact

Donald M. Curry
NASA Johnson Space Center
Houston, Texas 77058

Vuong T. Pham
NASA Johnson Space Center
Houston, Texas 77058

Ignacio Norman
Boeing North American, Inc.
Houston, Texas 77058

Dennis C. Chao
Boeing North American, Inc
Houston, Texas 77058

March 2000

Since its founding, NASA has been dedicated to the advancement of aeronautics and space science. The NASA Scientific and Technical Information (STI) Program Office plays a key part in helping NASA maintain this important role.

The NASA STI Program Office is operated by Langley Research Center, the lead center for NASA's scientific and technical information. The NASA STI Program Office provides access to the NASA STI Database, the largest collection of aeronautical and space science STI in the world. The Program Office is also NASA's institutional mechanism for disseminating the results of its research and development activities. These results are published by NASA in the NASA STI Report Series, which includes the following report types:

- TECHNICAL PUBLICATION. Reports of completed research or a major significant phase of research that present the results of NASA programs and include extensive data or theoretical analysis. Includes compilations of significant scientific and technical data and information deemed to be of continuing reference value. NASA counterpart of peer-reviewed formal professional papers, but having less stringent limitations on manuscript length and extent of graphic presentations.

- TECHNICAL MEMORANDUM. Scientific and technical findings that are preliminary or of specialized interest, e.g., quick release reports, working papers, and bibliographies that contain minimal annotation. Does not contain extensive analysis.

- CONTRACTOR REPORT. Scientific and technical findings by NASA-sponsored contractors and grantees.

- CONFERENCE PUBLICATION. Collected papers from scientific and technical conferences, symposia, seminars, or other meetings sponsored or co-sponsored by NASA.

- SPECIAL PUBLICATION. Scientific, technical, or historical information from NASA programs, projects, and missions, often concerned with subjects having substantial public interest.

- TECHNICAL TRANSLATION. English-language translations of foreign scientific and technical material pertinent to NASA's mission.

Specialized services that complement the STI Program Office's diverse offerings include creating custom thesauri, building customized databases, organizing and publishing research results ... even providing videos.

For more information about the NASA STI Program Office, see the following:

- Access the NASA STI Program Home Page at *http://www.sti.nasa.gov*

- E-mail your question via the Internet to help@sti.nasa.gov

- Fax your question to the NASA STI Help Desk at (301) 621-0134

- Telephone the NASA STI Help Desk at (301) 621-0390

- Write to:
  NASA STI Help Desk
  NASA Center for AeroSpace Information
  7121 Standard Drive
  Hanover, MD 21076-1320

NASA/TP—2000–209760

Oxidation of Reinforced Carbon-Carbon Subjected to Hypervelocity Impact

Donald M. Curry
NASA Johnson Space Center
Houston, Texas 77058

Vuong T. Pham
NASA Johnson Space Center
Houston, Texas 77058

Ignacio Norman
Boeing North American, Inc.
Houston, Texas 77058

Dennis C. Chao
Boeing North American, Inc
Houston, Texas 77058

March 2000

Acknowledgments

The authors wish to express their appreciation to Eric Christensen and Frankel Lyons of the JSC Hypervelocity Impact Technology Facility and J. D. Milhoan of the NASA JSC Atmospheric Reentry Materials and Structures Evaluation Facility for participating in and contributing to this work.

Contents

Tables

Figures

Contents

(continued)

Acronyms and Nomenclature

RCC	reinforced carbon-carbon
MOD	meteoroid/orbital debris
SiC	silicon-carbide
HVI	hypervelocity impact
HIT-F	Hypervelocity Impact Technology Facility
ARMSEF	Atmospheric Reentry Materials and Structures Evaluation Facility
IS&AG	JSC Image Science and Analysis Group
ISS	International Space Station

D_h - hole diameter, cm

d – Impacting particle diameter, cm

ρ_p – density of impacting particle, g/cm^3

V – particle velocity, Km/s

θ - impact angle, deg

P = pressure, lbf/ft^2

Po = atmosphere pressure (2116.2 lbf/ft^2)

IE = impact energy, ft-lbf

$\dot{D}_f$ = front coating hole diameter growth rate, in/sec

$\dot{D}_b$ = back coating hole diameter growth rate, in/sec

X1 = function of pressure defined in table 5

X2 = function of impact energy defined in table 5

X3 = function of pressure defined in table 5

X4 = function of impact energy defined in table 5

Abstract

This paper presents results from arc jet tests conducted at the NASA Johnson Space Center (JSC) on reinforced carbon-carbon (RCC) samples subjected to hypervelocity impact. The RCC test specimens are representative of RCC components used on the Space Shuttle Orbiter. The arc jet testing established the oxidation characteristics of RCC when hypervelocity projectiles, simulating meteoroid/orbital debris (MOD), impact the RCC material. In addition to developing correlations for use in trajectory simulations, we discuss analytical modeling of the increased material oxidation in the impacted area using measured hole growth data. Entry flight simulations are useful in assessing the increased Space Shuttle RCC component degradation as a result of impact damage and the hot gas flow through an enlarging hole into the wing leading-edge cavity.

Introduction

During the early flights of the Space Shuttle, micrometeoroids and orbital debris were not recognized as a significant hazard to the Orbiters. However, more recent models of the space environment suggest that MOD pose a significant threat to the orbital vehicle. The RCC wing leading edge and nose cap are especially vulnerable to this MOD environment and have been identified as areas of the Orbiter that appear to pose the highest risk for critical failure. Figure 1 presents the relative risk of the RCC as compared to the other Orbiter components.
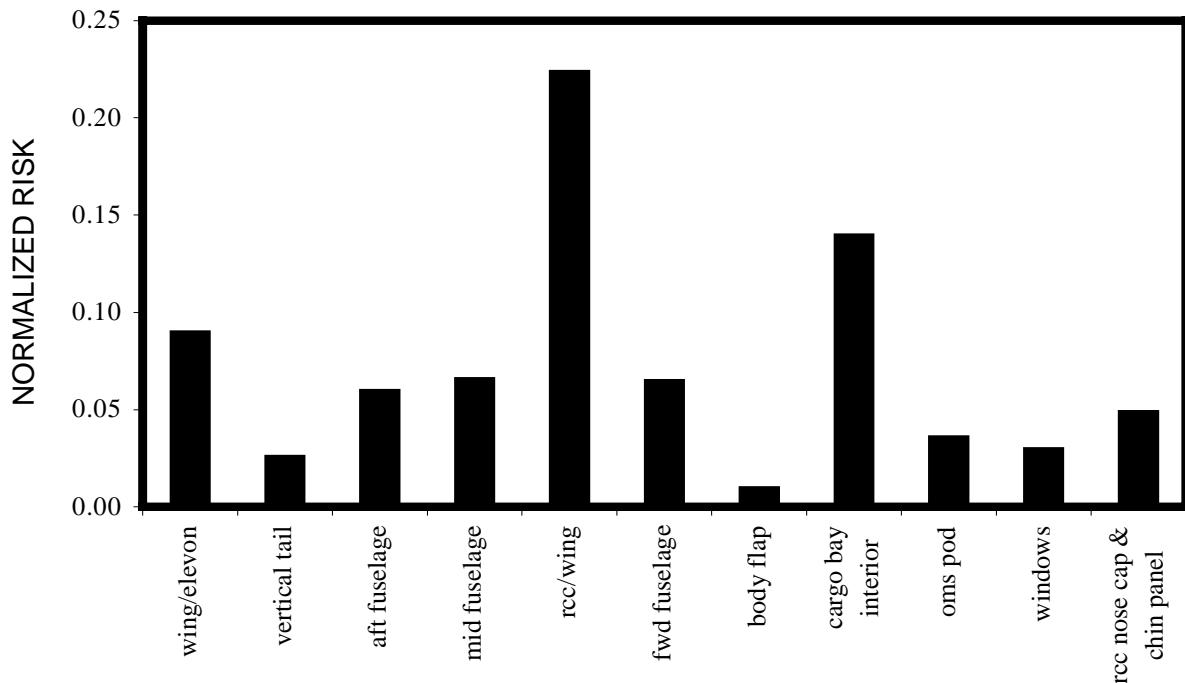

Figure 1. Meteoroid/orbital debris relative risks for various components using omnidirectional flux analysis.

1

Because RCC is a structural composite and because of the brittle nature of the RCC silicon carbide (SiC) coating and the requirement to maintain oxidation protection, the effect of impact damage on the mission life and structural performance of the RCC components is of concern. Impact damage may occur from a variety of threats with a wide range of impact speeds. Meteoroids and human-made orbital debris represent a source of high-velocity impact damage, while other sources of damage include launch debris, runway debris from landing, and handling and service damage. Orbital debris can impact orbiting spacecraft at velocities from less than 1 km/sec to over 14 km/sec, and meteoroids from 10 km/sec to over 70 km/sec.

The effects of hypervelocity impact damage on the oxidation performance on the RCC material has been investigated experimentally. Specifically, arc jet tests have been performed on RCC samples impacted at hypervelocity to establish oxidation performance and develop corrections for predicting the increased oxidation during a typical Orbiter entry. Hypervelocity impact testing produced "complete penetration" or "through-holes" in the test specimens. The arc jet tests were performed on RCC samples impacted at hypervelocity to establish the rate of enlargement of the "through-holes" due to oxidation. The hole growth rate was used to develop corrections for predicting the increased oxidation during a typical Orbiter entry. The typical entry hole growth rates can be used to calculate the hot gas influx into the wing leading-edge cavity through the resulting "burn through" hole and assess structural vehicle component damage. These hole growth correlations, along with the probabilities of impact damage, are used to assess MOD impacts on the Orbiter RCC vehicle components for the establishment of flight rules and initial impact hole acceptability criteria. The objective of this paper is to describe these tests, and present test results and correlations.

RCC Test Articles

Test articles consisted of SiC-coated RCC samples. Figure 2 shows the nominal dimensions of the coating and substrate that make up the 0.25-in.-thick RCC test samples. These samples are representative of RCC components on the Space Shuttle Orbiter, which include the nose cap, wing leading edge panels, an area between the nose landing gear door and nose cap, and a small area surrounding the forward attach fitting of the external tank to the Orbiter.
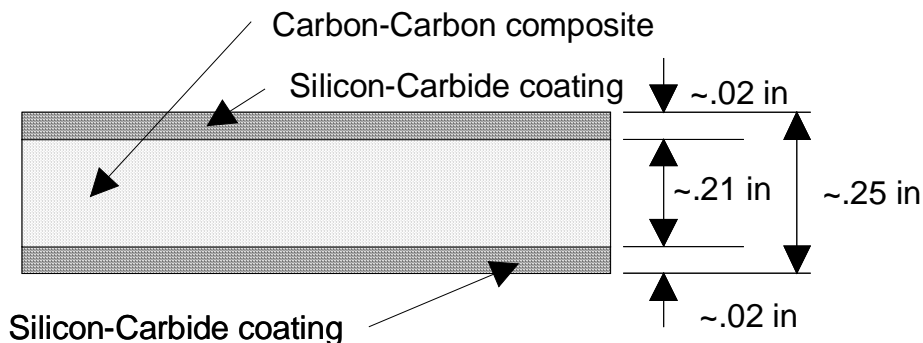

Figure 2. RCC test article dimensions (typical).

The test sample substrate is an all carbon composite laminate fabricated in a multiple pyrolysis and densification process from a 19-ply phenolic prepreg graphite lay-up. The substrate has a density of 90 lb/ft³ to 100 lb/ft³ and is typically 0.17 in. to 0.21 in. thick.

The oxidation-resistant SiC coating is formed in a diffusion reaction process. It is typically 0.02 in. to 0.04 in. thick. Further oxidation resistance is provided by impregnation with tetraethyl-orthosilicate that, when cured, leaves a silicon dioxide residue throughout the coating and substrate. Any surface porosity or micro cracks are filled by an application of a surface sealant (sodium silicate/SiC mixture) in the final step of the fabrication process. More details on the development and fabrication of the Orbiter RCC applications are given by Curry, et al.[1, 2]

Hypervelocity Impact Tests

Hypervelocity impact (HVI) testing of RCC was conducted at the JSC Hypervelocity Impact Technology Facility (HIT-F) from August 27, 1997 to November 21, 1997.[3] The HIT-F supported the testing by providing 24 tests investigating the effects of hypervelocity impacts of projectiles simulating MOD striking RCC.

Two types of targets were tested: ten flat plate 6-in. x 6-in. RCC target samples, and a curved surface sample used for pretesting and a full-scale RCC wing leading panel. All samples had a thickness of approximately 0.25 in. The primary objective of these tests was to impact each sample twice, with each impact producing a separate and complete penetration. Impact holes of .125 in., 0.25 in., or .375 in. diameter were produced. The samples had to be impacted by the HIT-F such that two circular disks measuring 2.8 in. in diameter with the impact hole in the center could be cut from each sample. This sample size was required to fit the specimen holders for arc jet testing. Data were collected in the HIT-F for correlation of projectile size to hole size. After each sample was tested in the HIT-F, it was sent to the JSC Arc Jet Facility.

The objective for testing the full-scale wing leading edge panel was to collect data for correlation of projectile size to the hole size through the top of the panel and the secondary damage that would occur to the internal and external bottom of the panel. There was an interest in what kind of secondary damage would occur to the wing spar insulation inside the wing leading edge panel. These results were reported separately in reference 3.

Previous hypervelocity impact testing conducted at JSC had established the threshold for several damage modes on coated RCC samples. Equations have been developed relating impact conditions to RCC damage, such as penetration depth and hole size.[4,5] An equation was developed to predict hole size when complete penetration of RCC occurs. This equation was used to predict the diameter/velocity required to create the three hole sizes used in this investigation. Figure 3 provides a comparison between predicted hole size and HVI data.

$$D_h = 2.20 \, d \, \rho_p^{1/3} \, (V \cos\theta)^{1/3} - 0.36$$

Where: D_h - hole diameter, cm
d – Impacting particle diameter, cm
ρ_p – density of impacting particle, g/cm^3
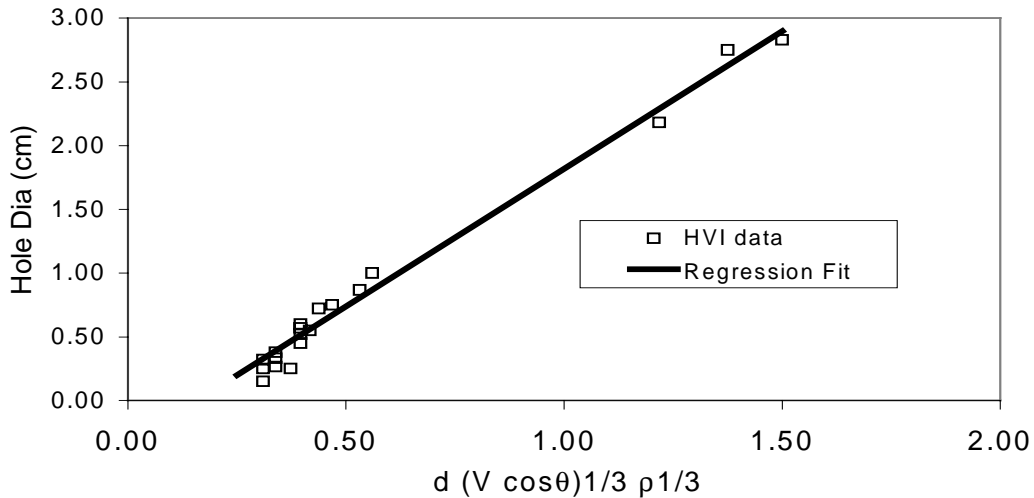V –particle velocity, km/s
θ - impact angle, deg

Figure 3. RCC hole size correlation.

Table 1 presents a summary of the impact test results, and figure 4 shows a representative photo of the target damage. Figure 4 shows the result of a 5/64-in.-dia. aluminum sphere impacting the 6-in. x 6-in. RCC sample at 6.63 km/sec normal to the surface. Because the SiC coating is brittle, the coating is damaged in an area around the impact site over 10 times larger than the projectile diameter. The hole through the specimen exposes the RCC substrate over an area 4 times larger than the projectile diameter. The graph in figure 5 illustrates the approximate front and back coating damage diameter as a function of impact energy. The coating on the rear side of the RCC is damaged in a wide area, larger than the front. Internal damage in the RCC substrate can extend significantly beyond the external damage that is readily detected by visual observation. Internal damage in the RCC consists of micro cracks and delaminations.

The hole diameters selected for producing the arc jet test specimens were of 0.125, 0.25, and 0.375 in., with kinetic energies of 50, 100, and 200 ft/lb, respectively.

The photographs presented in figures 6 and 7 represent the RCC front face impact damage as a result of 53 and 212 ft-lb of impact energy. Figures 8 and 9 show a photograph of the back face damage. These models are presented to illustrate the minimum and maximum energy levels used in the subject test program and the resulting RCC damage.

Table 1. Summary of Reinforced Carbon-Carbon Hypervelocity Test Results

JSC HIT-F Shot	Sample No.	Projectile Diameter Used*	Projectile Mass (mg)	Projectile Velocity (ft/s)	Projectile Velocity (km/s)	Projectile Kinetic Energy (J)	Projectile Kinetic Energy (ft-lb)	Through Hole Damage (Hole Size)	Front Diameter of Damage (in.)	Back Diameter of Damage (in.)
A3085	10.1	5/64"	12.39	21,195	6.46	258.53	190.69	9x9 mm	0.867	1.035
A3086	9.1	5/64"	11.65	22,508	6.86	274.12	202.19	9x9.5 mm	0.819	1.208
A3087	8.1	5/64"	11.53	21,753	6.63	253.41	186.92	9.5x9 mm	0.92	1.083
A3088	7.1	5/64"	11.62	22,639	6.90	276.61	204.03	9.5x9.5 mm	0.932	1.159
A3089	6.1	5/64"	11.70	23,033	7.02	288.29	212.64	9x9.5 mm	0.888	1.18
A3093	4.1	1/16"	5.86	22,278	6.79	135.09	99.64	6.5x6.5 mm	0.752	0.952
A3095	5.1	1/16"	5.68	23,098	7.04	140.75	103.82	6.5x7 mm	0.776	0.962
A3096	3.1	1/16"	5.82	23,262	7.09	146.28	107.9	6.5x7 mm	0.792	0.874
A3097	10.2	1/16"	5.67	22,803	6.95	136.94	101.01	6.5x6.5 mm	0.756	0.966
A3098	9.2	1/16"	5.97	23,361	7.12	151.32	111.61	6.5x6.5 mm	0.801	0.965
A3099	8.2	0.125 cm	2.81	23,361	7.12	71.23	52.54	3.5x3.5 mm	0.673	0.701
A3100	7.2	0.125 cm	2.92	23,033	7.02	71.95	53.07	3.5x3.5 mm	0.649	0.675
A3101	6.2	0.125 cm	2.85	23,295	7.10	71.83	52.98	4x4 mm	0.685	0.725
A3105	4.2	1/16"	5.28	23,197	7.07	131.96	97.33	6.5x6 mm	0.803	1.142
A3103	2.1	1/16"	5.71	23,000	7.01	140.29	103.48	6.5x6 mm	0.777	0.968
A3108	3.2	5/64"	11.61	23,000	7.01	285.26	210.41	hole-9.5x9 mm	0.913	1.069

*Commercially available sizes; projectile material Al2017-T4; projectile shape sphere; all impact angles are 0 deg (normal to the surface).

Figure 4. Typical posttest picture of a hypervelocity-impacted 6-in. x 6-in. RCC panel.
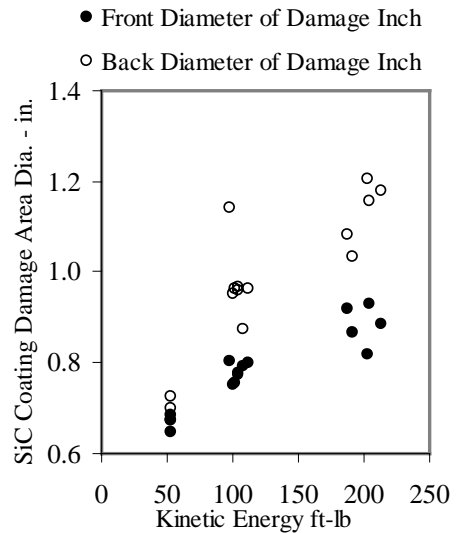

Figure 5. Hypervelocity impact energy vs RCC coating damage area.

5

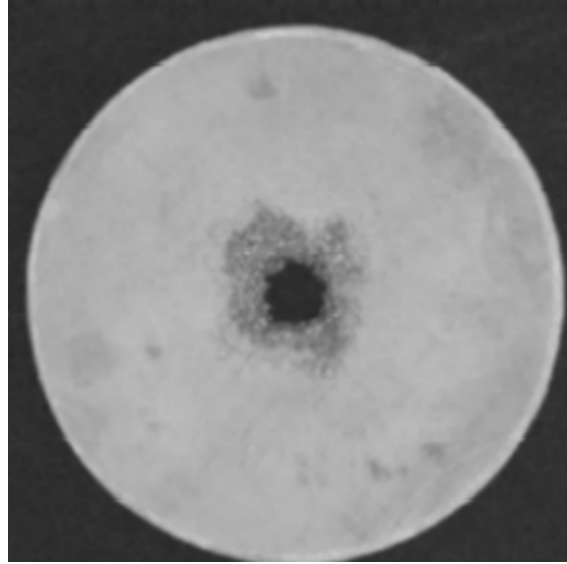**Figure 6. NASA model 1161 front face, pre arc jet test 53 ft-lb impact energy.**

Figure 7. NASA model 1152 front face, pre arc jet test 212 ft-lb impact energy.
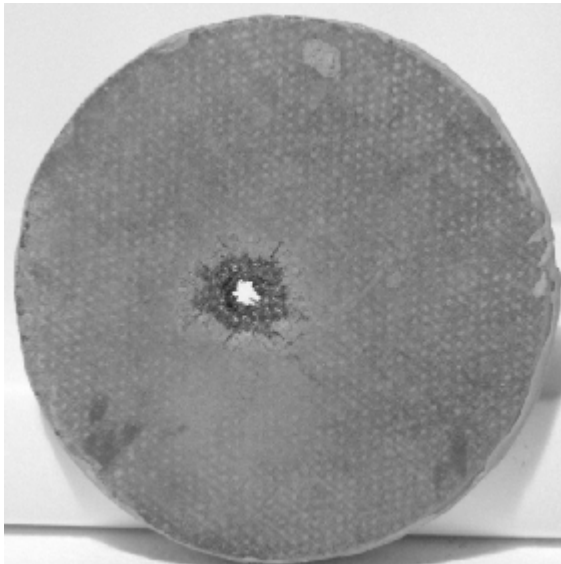

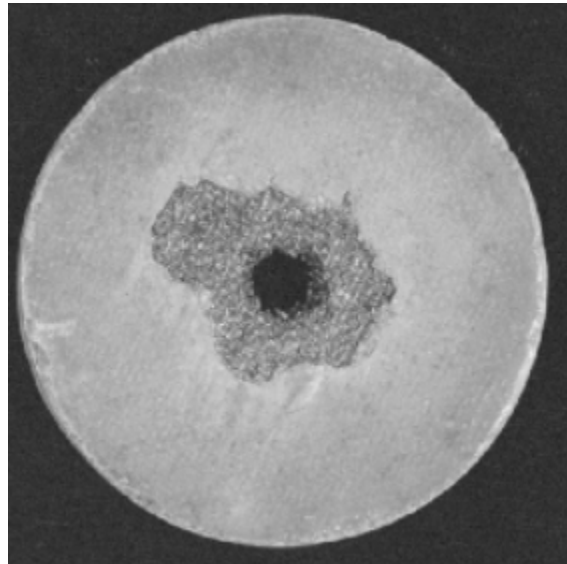**Figure 8. NASA model 1161 back face, pre arc jet test 53 ft-lb impact energy.**

Figure 9. NASA model 1152 back face, pre arc jet test 212 ft-lb impact energy.

Arc Jet Testing

The objective of the arc jet testing was to establish the oxidation characteristics of RCC with hypervelocity-impacted damage. RCC specimens were exposed to constant heating conditions for specific test points at temperature of 2500°F and 2800°F and pressures of 50 psf to 180 psf.

Test Facility and Conditions

This test program was conducted in JSC's Atmospheric Reentry Materials and Structures Evaluation Facility (ARMSEF). This facility simulates atmospheric entry conditions by heating test gas or gas mixtures electrically using a segmented, constricted, 10-megawatt direct current arc heater. For this test program, the gas mixture was nitrogen and oxygen to simulate air. Once the air was heated to a high-energy (high-enthalpy) level inside the arc heater, it was then expanded supersonically through a conical nozzle, which has a 5-in. diameter at the exit plane. The high-enthalpy and supersonic flow field is formed and then captured by a downstream supersonic diffuser. Inside the chamber, a hydraulic model insertion system permits the test articles to be located outside the flow field until the required test conditions have been established. Model insertion and retraction are normally performed within 1 sec from the command signal, thereby producing a step pulse heating profile on insertion and an immediate cessation of oxidation upon retraction. During the test, the chamber static pressure was maintained below 400 microns of Hg by a four-stage steam ejector system.

The facility data acquisition system obtained facility and test article data at a rate of 10 Hz. Surface temperature was monitored by a 0.865-micron optical pyrometer aimed in such a way that the entire field of view was covered by the specimen in the area between the hole and the edge of the specimen. Once the hole starts to grow, the exposed and burning carbon substrate will affect the measurements. Because of the potential erroneous surface temperature feedback, the test runs were made with constant arc heater parameters as identified in the calibration runs.

Two super-VHS video cameras were mounted outside on the test chamber. One was used to visually monitor and record the test articles' surfaces for transient hole diameter measurements. The other was used to monitor the flow field and the overall interior of the test chamber.

The arc jet test specimens were fabricated from a 6-in. x 6-in. panel that was first impacted at the appropriate energy level to produce a desirable hole diameter. The sample was then cut to approximately 2.8 in. diameter with the impacted hole at the center to make an arc jet test specimen. Test specimens were cut from an impacted panel using a high-power CO_2 laser. One of the benefits from the laser cutting was the melted SiC coating deposited on the exposed carbon edge, which acted as another oxidation protection layer. Once a specimen is cut from a panel, four small retention pin holes about 1/8 in. diameter and about 1/8 in. deep were drilled at 90 deg apart on its exposed carbon edge. The entire exposed carbon edge was then repaired with a mixture of Sermabond 487 and 1000 Grit SiC powder that was cured by heating to 300°F in air.

A sketch of the test specimen holder used during these tests is shown in figure 10. This figure shows the 2.0-in.-diameter hole through which gases ingested through the impact holes can pass without restriction. Ceramic rods support the holder such that a water-cooled conical interface block may smoothly divert the flow. The outlet slot between the holder and interface block has an area that is over 15 times that of the largest posttest impact hole area. Since the pressure just outside the slot is less than 0.6 psf, sonic conditions are maintained at the impact hole with large margin. In addition the stagnation pressure measurement at the forward end of the conical flow diverter indicated that sonic conditions existed at the impact holes.
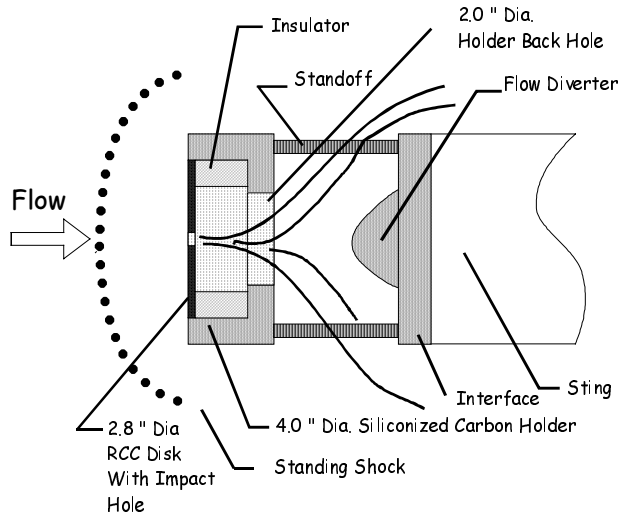

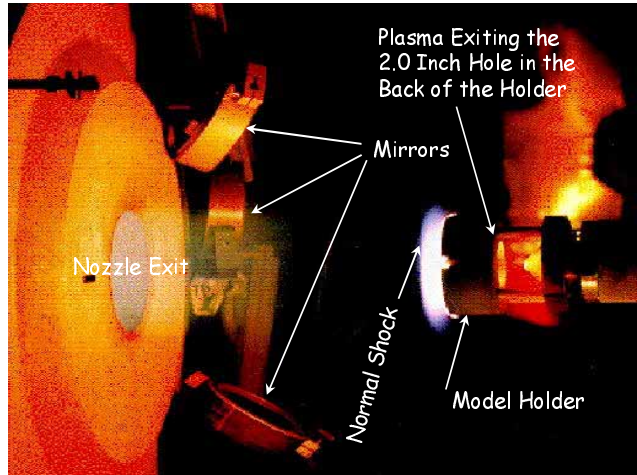**Figure 10. Test specimen holder test configuration.**

Figure 11. Specimen in chamber during test.

A view of one of the fixtures during the arc jet test is presented in figure 11. This photograph shows the normal shock in front of the specimen and the flow of ingested gases out the rear of the fixture. The arc jet nozzle, plasma flow field glow and the mirrors that are used to record the specimen face during testing are visible.

Test conditions were established by measuring the temperature of an undamaged specimen with an optical pyrometer that has repeatedly agreed to within 35°F with imbedded thermocouples in RCC calibration specimens (during many test programs over the last five years). The test specimens were exposed to constant heating conditions that were established with the undamaged specimens. No attempt was made to adjust to target temperatures, since the presence of the impact damage was expected to change the temperature measurement. Facility operating parameters such as current, voltage, test gas flow rate, oxygen percentage, chamber pressure, arc column pressure, energy balance enthalpy, and gas injection manifold pressure were recorded during the calibration test and monitored for repeatability during subsequent tests. The arc jet test facility parameters used in this test program were air mass flow rate, $\dot{m}$ = 0.2 - 0.7 lbm/sec; heater current, i = 530 - 1175 amps; and bulk enthalpy, h = 2400 - 7200 BTU/lbm.

A video camera mounted outside the chamber viewed each model indirectly through a window with the use of a small mirror mounted to one side of the exit nozzle of the plasma source. Since the models faced directly into the plasma flow field, they were seen obliquely in the mirror, making the circular articles and the holder appear elliptically shaped. The test specimen surface was videotaped before and after each test and during the tests by viewing through a first surface mirror at an angle of approximately 45 deg. These recordings are stored in the facility and are available for viewing. Posttest photographs with back lighting to emphasize the outlines of the penetration holes were taken for each test.

Specimen weights were taken to help assess substrate mass loss. It should be understood that erosion of the substrate and the SiC repair at the periphery and the erosion of SiC coating near the impact hole could affect the interpretation of these data.

Results

Fourteen arc jet tests were performed and are summarized in table 2. This table identifies the test conditions assigned to each specimen, impact energy sustained, the approximate level of visible pretest damage, arc jet exposure test time and conditions, and post arc jet test dimensions of the hole growth.

Figures 12A and 12B present the front and back pre arc jet exposure test photographs of specimen NASA #1159, typical test specimen. It can be noted of the coating damage, which resulted from the hypervelocity impact and penetration, that the backside damage has a larger spalled coating area than the front face coating spallation area. The specimen NASA #1159 was exposed to 2500°F, 50 psf for 450 sec.

Photographs of this typical posttest specimen (figures 12A-E) show the oxidation and growth of the impacted frontal area (12C) and of the backside area (12D) that occurred during the arc jet test. The hole growth of the test specimen grew by the oxidation of the exposed carbon-carbon substrate. Hole growth as a result of coating loss was not expected as there is negligible coating loss for temperatures between 2800°F - 3000°F for the Orbiter leading edge RCC.[7]

Figure 12E presents an oblique view of NASA specimen #1159, where it can be seen that there was additional substrate loss that formed a dishing out of the carbon sandwiched between the SiC front and back coating.

Figure 13A and 13B present the pre arc jet exposure test photograph of specimen NASA #1151 that can be compared with the post arc jet exposure photograph shown in views 13C and 13D. For this test condition (2800°F and 100 psf) there was significant front face coating erosion. In general, the front face of the damaged region grew faster than the backside of the specimen giving the hole a conical shape that is typical of all the 2800°F tests.
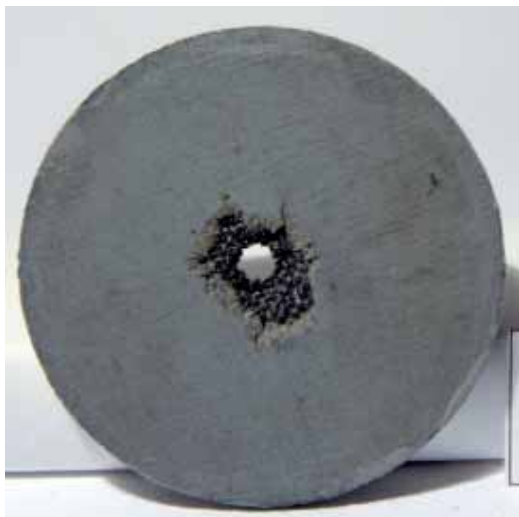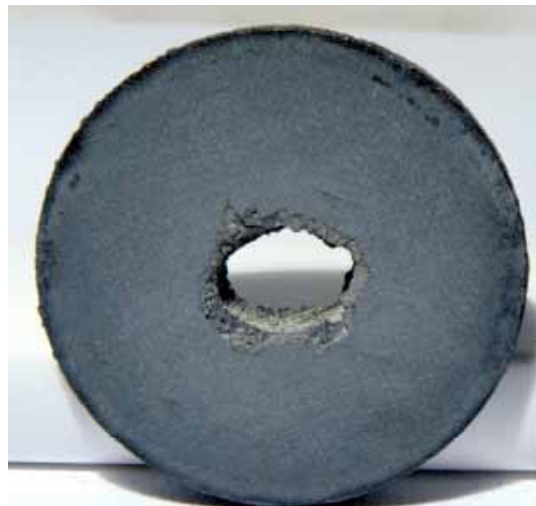
View 12A. Frontside pre arc jet.
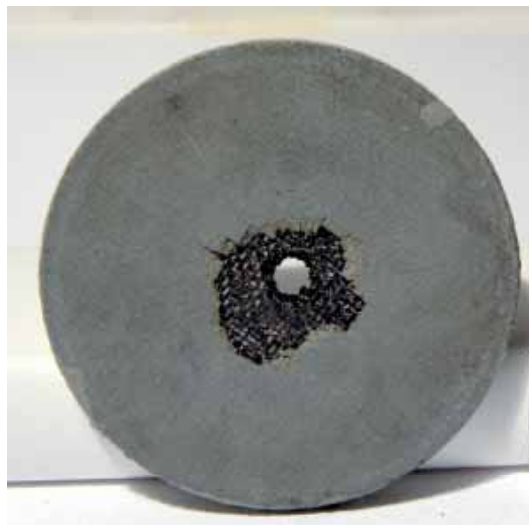
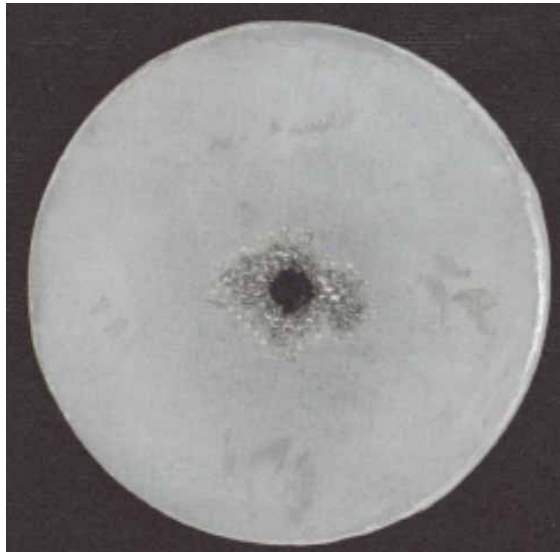View 12B. Backside pre arc jet.

View 12C. Frontside post arc jet.

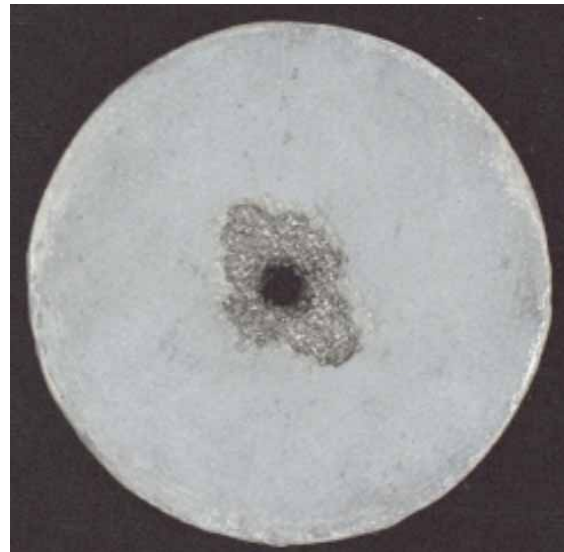

View 12D. Backside post arc jet.
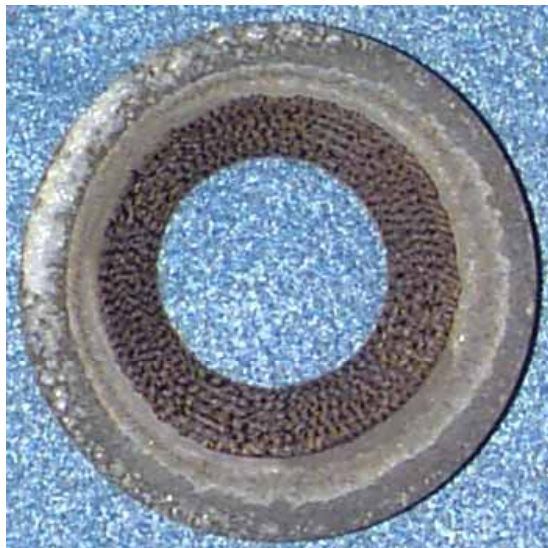

View 12E. Post arc jet test oblique.

**Figure 12. Hypervelocity impact damage
pre and post arc jet test 2500°F / 50 psf
model # 1159.**

View 13A. Frontside.

View 13B. Backside.

View 13C. Frontside.

View 13D. Backside.

Figure 13. NASA/JSC model #1151 pre and post arc jet exposure 2800°F/100 psf.

Table 2. RCC Orbital Debris Arc Jet Test Program Hole Growth Summary

JSC Arc Jet ID #	Panel # / Shot #	Targeted Hole Diameter [in.]	Test Conditions (°F/psf/s)	Impact energy (ft-lb)	Pretest Measurements			Posttest Measurements	
					Average Hole Diameter [in.]	Front Coating Diameter [in.]	Back Coating Diameter [in.]	Front Hole Dimensions [in.]	Back Hole Dimensions [in.]
1161	8.2	0.125	2800/100/450	52.54	0.138	0.673	0.701	1.525-1.621	0.992-1.043
1166	7.2	0.125	2800/50/450	53.07	0.138	0.649	0.675	1.003-1.056	0.642-0.659
1165	6.2	0.125	2800/180/450	52.98	0.157	0.685	0.725	0.652-0.744	0.390-0.491
1157	5.1	0.250	2500/180/450	103.82	0.266	0.776	0.962	0.552-0.653	0.680-0.769
1151	4.1	0.250	2800/100/450	99.64	0.256	0.752	0.952	1.890-1.909	1.216-1.233
1158	3.1	0.250	2800/50/450	107.9	0.266	0.792	0.874	1.249-1.309	0.853-0.862
1160	10.2	0.250	2800/180/450	101.01	0.256	0.756	0.966	0.948-1.136	0.670-0.764
1159	9.2	0.250	2500/50/450	111.61	0.256	0.801	0.965	0.476-0.721	0.607-0.778
1145	10.1	0.375	2500/50/450	190.69	0.354	0.867	1.035	0.691-0.762	0.799-0.809
1144	9.1	0.375	2800/180/150	202.19	0.364	0.819	1.208	1.010-1.064	0.677-0.680
1143	8.1	0.375	2500/180/450	186.92	0.364	0.92	1.083	0.741-0.811	0.846-0.885
1142	7.1	0.375	2800/100/408	204.03	0.374	0.932	1.159	1.941-1.978	1.240-1.257
1152	6.1	0.375	2800/180/304	212.64	0.364	0.888	1.18	1.350-1.503	1.091-1.120
1172	3.2	0.375	2800/50/450	210.41	0.364	0.913	1.069	1.423-1.437	0.989-1.002

The JSC Image Science and Analysis Group (IS&AG) used videotapes of each test to make an assessment of the hole growth (Appendix A).[6] Dimensional measurements of the diameters of both the larger front face of each hole (called the outer hole) and the back face of the each hole (called the inner hole) were made for 14 tests. Appendix A contains photographs for time cuts that are typical for the videotape images used by the IS&AG group to determine the raw data inner and outer hole growths. The minimum uncertainty in the diameter measurements is estimated to be 0.01 in. The minimum uncertainty applies only when the hole edge is well defined, focus is good, and there is no residual SiC to interfere with the edge identification, generally true for inner hole edge only. Outer edge uncertainty is .03 to .05 in. because of the appearance of new oxidizing (burning) rings of SiC. As these new rings glow brightly their edge blurs the image, giving a false image width. Typical hole diameter measurements as a function of time that the JSC IS&AG made for the 14 test articles are shown in figures 14 (2500°F) and 15 (2800°F).
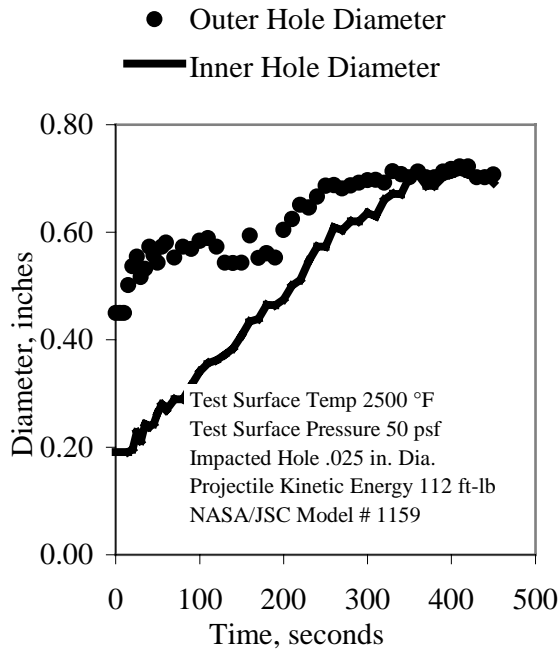
Figure 14. Video hole growth data for a 2500°F/0.25-in.-dia. impacted hole.
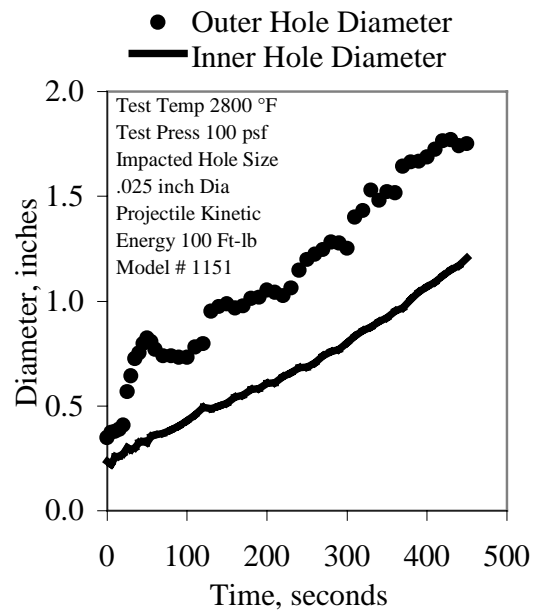

Figure 15. Video hole growth data for a 2800°F/0.25-in.-dia. impacted hole.

Hole growths for the 2500°F tests showed only loss of the RCC substrate and no visible SiC coating loss; thus the 2500°F hole growth was circular on the exposed substrate with virtually no difference in the outer and inner diameter.

Hole growths of the 2800°F test specimens developed a conical shape when viewed in cross section. The widest hole cone was formed by the 100-psf test cases, and the narrowest cone slopes were formed by the test cases tested at 180 psf. The conical hole shape phenomena is illustrated in figure 16. The test data are grouped to show the conical shape (outer ring diameter minus inner ring diameter).

The hole growth data derived from the assessments of the videotapes of arc jet testing, the test measurements made at the Hypervelocity Lab, and the measurements performed at the ARMSEF were used for final hole growth prediction methods.
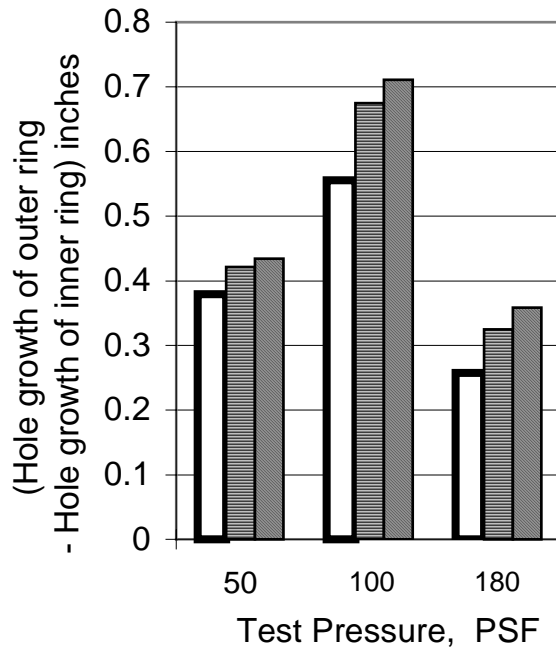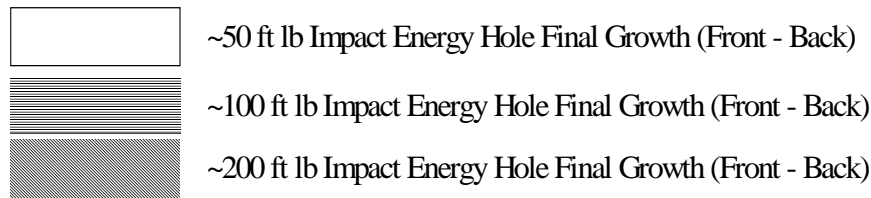
Figure 16. Conical shape of hole growth at 2800°F.

Test Data Analysis and Correlation

2500°F Tests

Test data from the 2500°F series indicated that early in the test period the front hole growth rate was much higher than the back hole. Approximately 200 sec into the test the back hole diameter becomes equal to the front hole diameter and the hole growth stopped. The results of comparisons between the pretest and posttest test specimens indicated the final hole size is either equal or less than the initial size of the front coating damage area (the coating was either broken into pieces or spalled) caused by the hypervelocity impact test. There is no coating oxidation at 2500°F; thus the hole growth was limited to the size of the impact damaged area (i.e., exposed bare substrate, figure 12).

Comparisons between these test data and the RCC substrate mass loss correlation (developed from the test data of non-impacted and non-coated RCC[7]) predictions show that the actual mass loss rate is around two to four times higher than predicted. However, the mass loss rate has no significant relationship with the level of the impact energy except that the final size of the hole is proportional to the level of the impact energy. The higher impact energy causes more coating damage, coating removal, and substrate exposure. The results of the data analysis for the 2500°F test data group are shown in table 3.

Table 3. Substrate Mass Loss of Hypervelocity Impacted RCC for the 2500°F Tests

Test Specimen JSC ID	Pressure psf	Impact Energy ft-lb	Damage Hole Initial Diameter (in)	Damage Hole Final Diameter PTM (in)	*Ratio Final Hole Growth	RCC Substrate Mass Loss Post Test Measurement lbm/sec-sq ft
1145	50	190	0.354	0.656	1.85	3.605E-03
1143	180	186	0.364	0.672	1.85	3.635E-03
1159	50	111	0.256	0.594	2.32	4.050E-03
1157	180	103	0.266	0.531	2.00	3.466E-03

*Ratio = final hole diameter / initial hole diameter

Test Specimen JSC ID	Pressure psf	Impact Energy ft-lb	Front Hole Diameter VTD inches	RCC Substrate Loss Rate VTD lbm/sec-sq ft	RCC Substrate Loss Rate PRD lbm/sec-sq ft	MLR_{PTM} /MLR_{PRD}	MLR_{VTD} /MLR_{PRD}
1145	50	190	0.649	3.553E-03	8.784E-04	4.1	4.05
1143	180	186	0.600	3.058E-03	1.667E-03	2.18	1.83
1159	50	111	0.605	4.123E-03	8.784E-04	4.61	4.69
1157	180	103	0.529	3.449E-03	1.667E-03	2.08	2.07

MLR = RCC Substrate Mass Loss Rate   PRD = Correlation Prediction (w/o an impacted hole)
PTM = Posttest Measurement   VTD = Video Test Data at 200 sec after Test

2800°F Tests

Test data from the 2800°F series showed that the characteristics of the holes are quite different from the 2500°F series. The holes from the 2500°F test are irregular in shape but keep a shape similar to one resulting from the impact test (figure 12). The holes from 2800°F are large, round shapes with a significant difference in size between the front hole and back hole diameters (figure 13).

Inspection of the test specimen after the impact test and before the arc jet thermal test indicates that the through-hole diameter from the front to the back is about the same size with circumferential damage/delamination of the hole wall surface. Upon insertion of the test specimen into the arc jet stream, the diameter of the front face surface hole increases much more than the back surface. This phenomenon can be seen from the video test data illustrated in Appendix A.

The 2800°F test series included three different levels of impact energy and three different pressure environments. Based on these test data, correlations of an impacted RCC hole growth as a function of the level of impact energy and pressure were developed. The correlations assumed a constant hole growth rate with respect to time. Plots of the test data and the constant hole growth rate line are shown in Appendix B. Since the front and back hole growth rates are different, the development of the correlations for the front and back hole growths were performed separately. A typical plot of the test data and the assumed constant hole growth rate is shown in figure 17.

Development of an impacted RCC hole growth correlation proceeds in two phases. In phase one, 18 constants of the hole diameter growth rates—9 for the front end of the hole and 9 for the back of the hole—were established based on the test data of 9 different test conditions. These growth rates are shown in table 4. With these growth rates, two correlations were developed: one for the growth rate as a function of the level of impact energy and the other for the growth rate as a function of pressure ratio (the test pressure divided by atmospheric pressure). These two correlations were then used as the second-generation independent variables and a regression analysis was performed. The final correlations are shown in table 5. As the correlations indicate, the effect of the pressure environment on the hole growth rate is a second-order polynomial curve and the effect of the impact energy on the hole growth rate is a power curve.
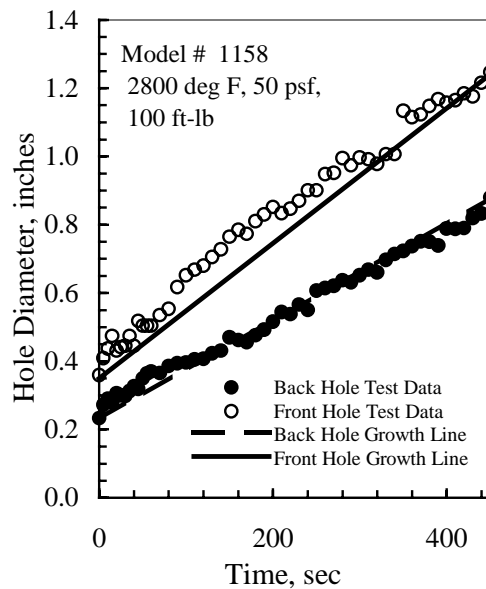
Figure 17. Front and back hole growth rate comparison.

Figures 18 to 21 show a comparison of the test data and predictions, using the correlations, for both front and back coating hole growth rates, and illustrate the effects of impact energy and pressure on hole growth. As expected with increasing impact energy, the hole growth rate increases as a result of coating and substrate damage. As the arc jet test pressure was increased from 50 to 180 lb/ft^2, hole growth increased as the pressure change from 50 to 100 lb/ft^2, but then decreased at a pressure

16

of 180 lb/ft^2. This reduction in hole growth is a result of a passive glassy layer (SiO$_2$) being formed on the carbon surface, since the carbon substrate has been impregnated with tetraethyl-orthosilicate as part of the RCC oxidation protection system.

Table 4. An Impacted RCC Hole Growth Rate [Correlated From Test Data]

Impact Energy ft-lb	Pressure psf	Temperature °F	Hole Diameter Growth Rate in./sec
(A) Front Coating Hole			
50	50	2800	1.68-03
50	100	2800	3.04E-03
50	180	2800	1.20E-03
100	50	2800	1.98E-03
100	100	2800	3.24E-03
100	180	2800	1.80E-03
200	50	2800	2.01E-03
200	100	2800	3.20E-03
200	180	2800	1.82E-03
(B) Back Coating Hole			
50	50	2800	1.36E-03
50	100	2800	1.96E-03
50	180	2800	1.18E-03
100	50	2800	1.44E-03
100	100	2800	2.18E-03
100	180	2800	1.73E-03
200	50	2800	1.64E-03
200	100	2800	2.36E-03
200	180	2800	1.93E-03

Front Hole Prediction, IE = 50 ft-lb
Front Hole Prediction, IE = 100 ft-lb
Front Hole Prediction, IE = 200 ft-lb
● Front Hole Test Data, IE = 50 ft-lb
◆ Front Hole Test Data, IE = 100 ft-lb
□ Front Hole Test Data, IE = 200 ft-lb
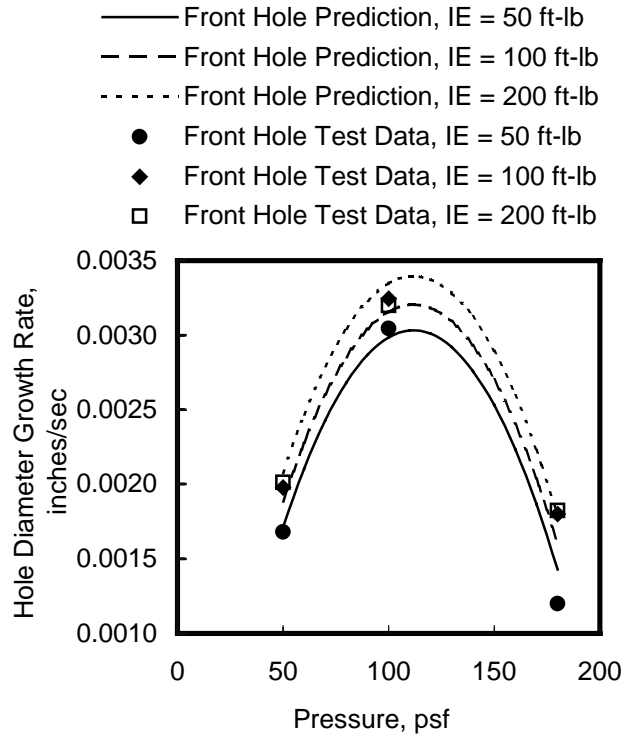
Figure 18. Comparison of test data and predictions for front hole growth rate (pressure).

Front Hole Prediction, P=50 psf
Front Hole Prediction, P=100 psf
Front Hole Prediction, P=180 psf
● Front Hole Test Data, P=50 psf
◆ Front Hole Test Data, P=100 psf
□ Front Hole Test Data, P=180 psf
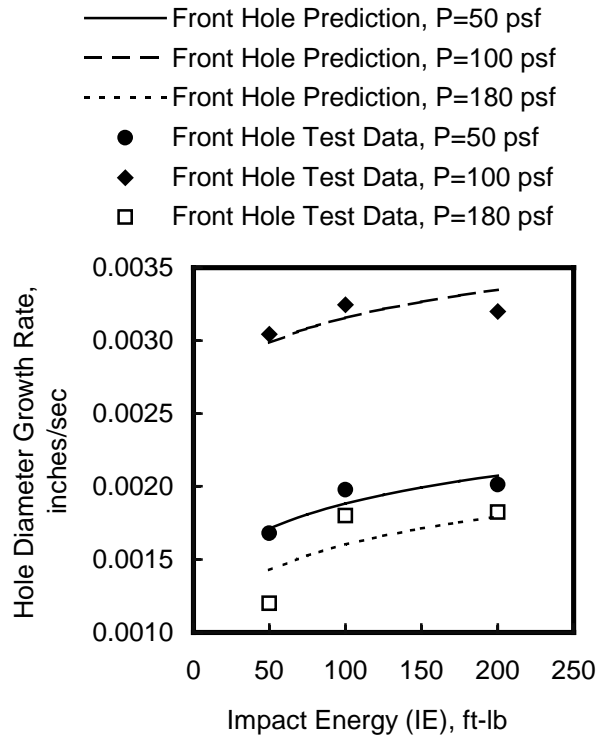
Figure 19. Comparison of test data and predictions for front hole growth rate (impact energy).

18
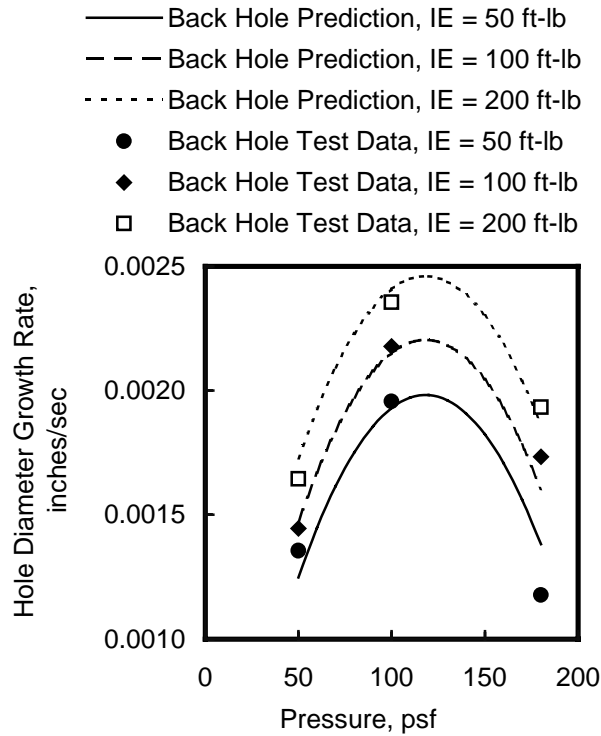
Figure 20. Comparison of test data and predictions for back hole growth rate (pressure).
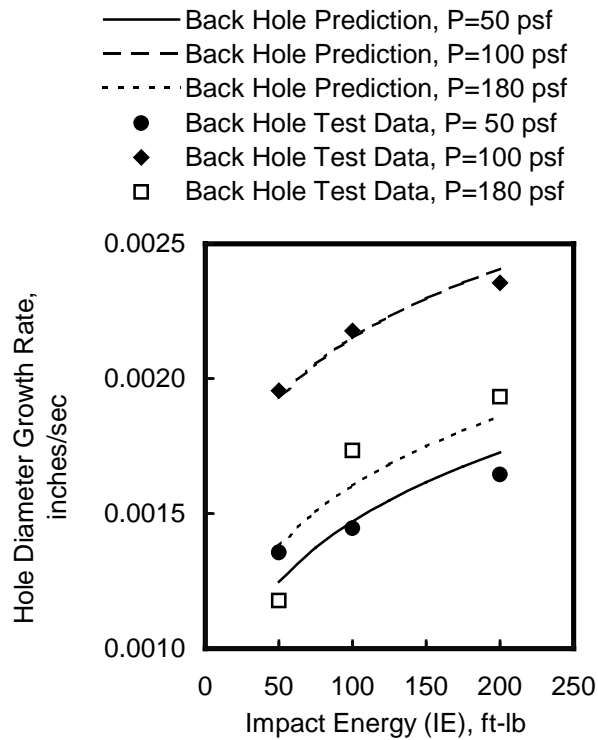
Figure 21. Comparison of test data and predictions for back hole growth rate (impact energy).

Table 5. Correlations for an Impacted RCC Hole Growth

> Correlation for the Front Coating Hole Growth Rate:
>
> $$\dot{D}_f = -0.00168398 + X1 + 0.794886\ (X2)$$
>
> Where $\dot{D}_f$ = Front Coating Hole Diameter Growth Rate, in/sec
>
> $X1 = -1.54763 \left(\dfrac{P}{Po}\right)^2 + 0.163622 \left(\dfrac{P}{Po}\right) - 1.11310E\text{-}3$
>
> $X2 = 1.02886E\text{-}3\ (IE)^{0.156}$
> P = Pressure, psf
> Po = 1 atm (2116.2 psf)
> IE = Impact Energy, ft-lb
>
> Correlation for the Back Coating Hole Growth Rate:
>
> $$\dot{D}_b = -0.00164586 + (X3) + 0.953631\ (X4)$$
>
> Where $\dot{D}_b$ = Back Coating Hole Diameter Growth Rate, in/sec
>
> $X3 = -7.05562E\text{-}1 \left(\dfrac{P}{Po}\right)^2 + 7.88547E\text{-}2 \left(\dfrac{P}{Po}\right) + 1.22376E\text{-}5$
>
> $X4 = 6.50434E\text{-}4\ (IE)^{0.210369}$

Application to Flight

The correlations developed from this test program only cover two temperature points, 2500°F and 2800°F. To perform a flight simulation requires a range of temperatures, from 500°F to 3000°F. Therefore, the following assumptions were made:

1. The mass loss correlation developed from the current 2500°F test data for substrate mass loss will hold for the temperature range of 500°F to less than 2800°F (this correlation is in a form of factors of the RCC substrate mass loss correlations developed from the test data of nonimpacted and noncoated RCC).

2. There is no coating mass loss in the temperature range of 500°F to less than 2800°F (this was concluded from a previous RCC over-temperature test program[7]). Therefore, during the flight while the temperature is below 2800°F, the hole will only grow up to the size of the impacted coating damage area.

3. At the temperature range of 2800°F to 3000°F, the coating mass loss rate remains a constant with respect to the temperature (again, this was concluded from a previous RCC over-temperature test program[7]), and the mass loss/hole growth rate correlations developed from the current 2800°F test data will hold throughout this temperature range. Based on these assumptions, plus the new correlations, a flight simulation program was developed for the flight application.

Assessment of an entry environment using the methodology developed begins with a thermal entry analysis for the entire RCC leading edge subsystem. A typical International Space Station (ISS) Shuttle mission trajectory case R, 233K forward cg with 57 deg inclination was chosen. Figure 22 presents the temperature histories that represent the entire wing leading edge. For this assessment of the RCC wing leading edge areas where temperatures are predicted to be below 2800°F, the hole growth is not expected to expand beyond the coating damage surrounding the impacted hole. An examination of RCC temperatures reveal that only panels 8, 9, and 10 stagnation area would experience entry temperatures above 2800°F where major coating erosion would be predicted. The entry environment for panel 9 stagnation area is presented in figure 23.

The assessment of the impact damage area of the wing leading edge panel requires the prediction of the expected hole growth history. This hole growth history is used to evaluate the consequences of the potential damage effects to the Orbiter structure. For this example a 0.25-in.-dia. hole resulting from MOD impact was assumed. Figure 24 presents the predicted hole growth history for the ISS Case R trajectory. The back hole growth rate is used to calculate the hot gas influx into the wing leading edge cavity for assessing wing spar insulation and structural damage. Final hole diameter of 1.76 and 1.415 in., respectively, for the front and back surfaces is predicted.
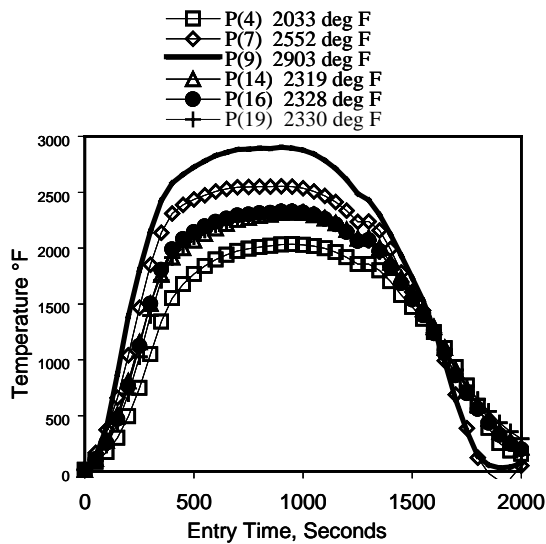
Figure 22. Temperature histories for the stagnation area of the wing leading edge panels 4, 7, 9, 14, 16, and 19 for the ISS mission case R 233K, 57-deg inclination entry trajectory.
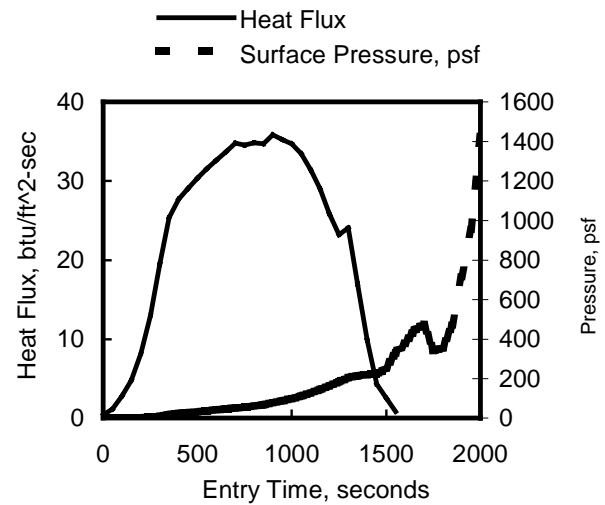
Figure 23. Heat flux and pressure history for the stagnation area of the wing leading edge panels 9 ISS mission case R 233K, 57-deg inclination entry trajectory.
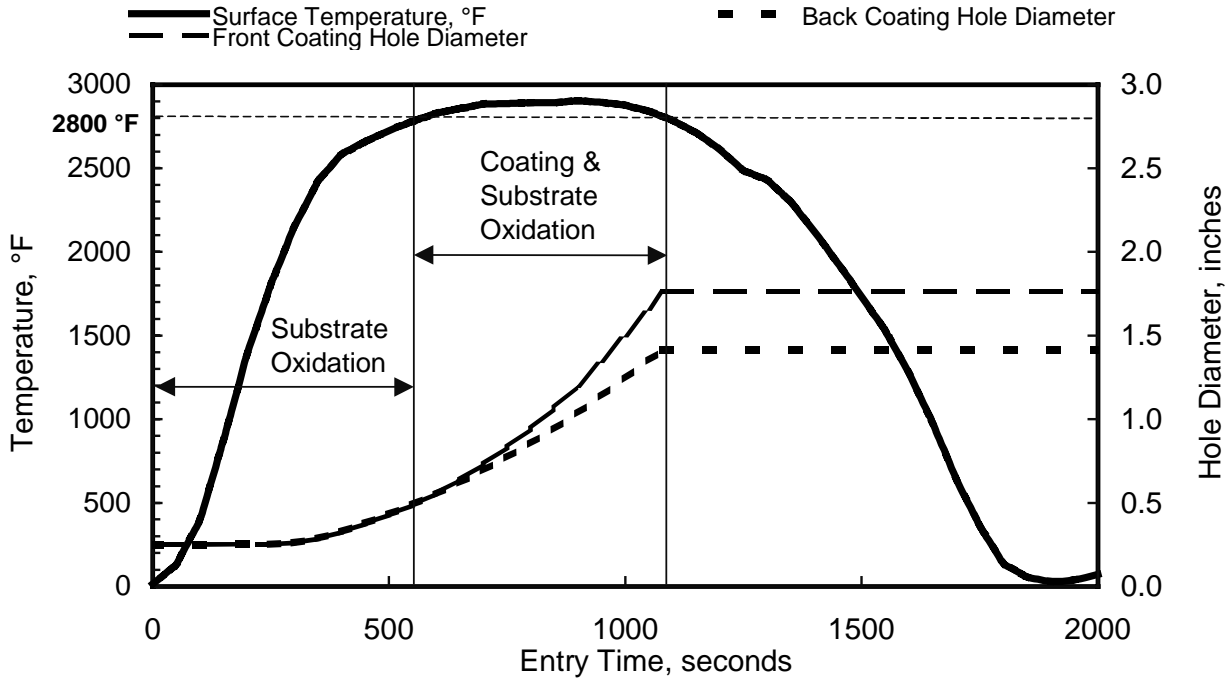
Figure 24. RCC hole growth history for ISS case R, entry trajectory.

Concluding Remarks

This report presented results from arc jet tests conducted on hypervelocity impacted RCC test specimens and hole growth rates measured with video techniques and posttest examinations. Included were correlations developed for both front face and back face mass loss as a function of hypervelocity impact energy, pressures, and two test temperatures, 2500°F and 2800°F. An assessment of a typical entry with an assumed impact damage to estimate hole growth was included. These correlations, along with the probabilities of impact damage, can be used to assess MOD impacts on the Orbiter RCC and hot gas flux though an enlarging hole with resultant impingement on the internal insulation components.

References

1. Curry, D. M., Scott, H. C., and Webster, C. N., Material Characteristics of Space Shuttle Reinforced Carbon-Carbon, Proceedings of 24th National SAMPE Symposium, Volume 24, Book 2, 1979, pp. 1524-1531.

2. Dotts, R. L., Curry, D. M., and Tillian, D. J., Orbiter Thermal Protection System, Space Shuttle Technical Conference, NASA CP-2342, Part 2, 1983, pp. 1062-1081.

3. Lyons, Frankel, Hypervelocity Impact Testing of Reinforced Carbon-Carbon (RCC), NASA JSC 28398, May 1998 (internal publication; contact author for documentation).

4. Christiansen, E. L., Curry, D. M., Kerr, J. H., Cykowski, E., and Crews, J. L., *Evaluation of the Impact Resistance of Reinforced Carbon-Carbon*, Proceedings of the Ninth International Conference of Composite Materials, Madrid, Spain, 1993.

5. Christiansen, E. L. and Friesen, L. *Penetration Equations for Thermal Protection Materials*, International Journel of Impact Engineering, Vol. 20, 1997, pp. 153-164.

6. Gaunce, M., *Assessment of Orbital Debris Test Hole Growth*, NASA Memo SN3-98-009, March 24, 1998.

7. Williams, S. D., Curry, Donald M., Chao, Dennis C., and Pham, Vuong T., *Ablation Analysis of the Shuttle Orbiter Oxidation Protected Reinforced Carbon-Carbon* AIAA Journal of Thermophysics and Heat Transfer, Volume 9, No.3, July–September, 1995, pp. 478–485.

Appendix A

ARMSEF Orbital Debris Arc Jet Tests

Hole Growth Measurements

JSC Image Science and Analysis Group
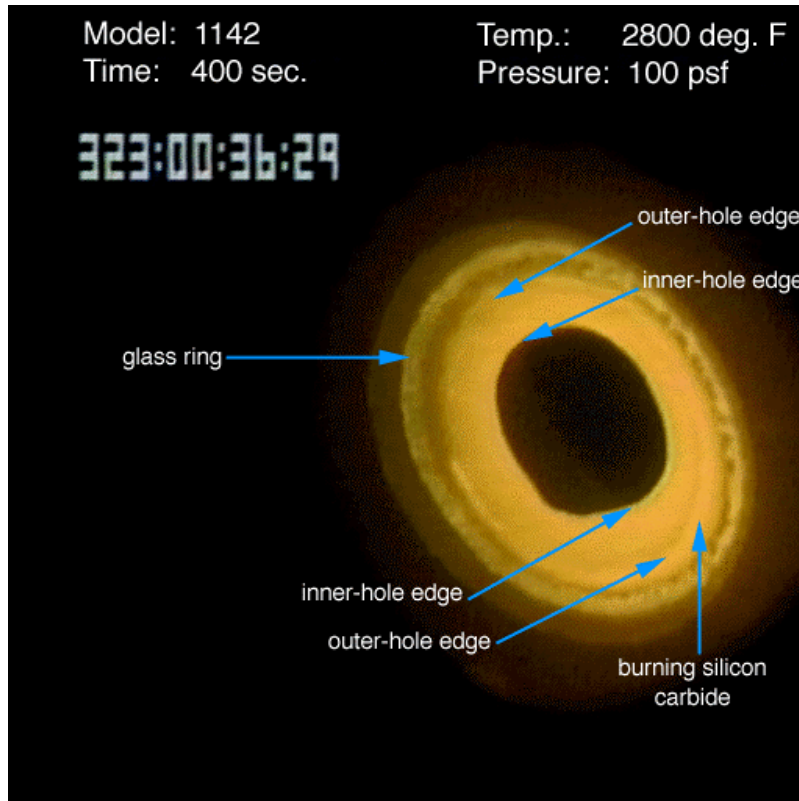
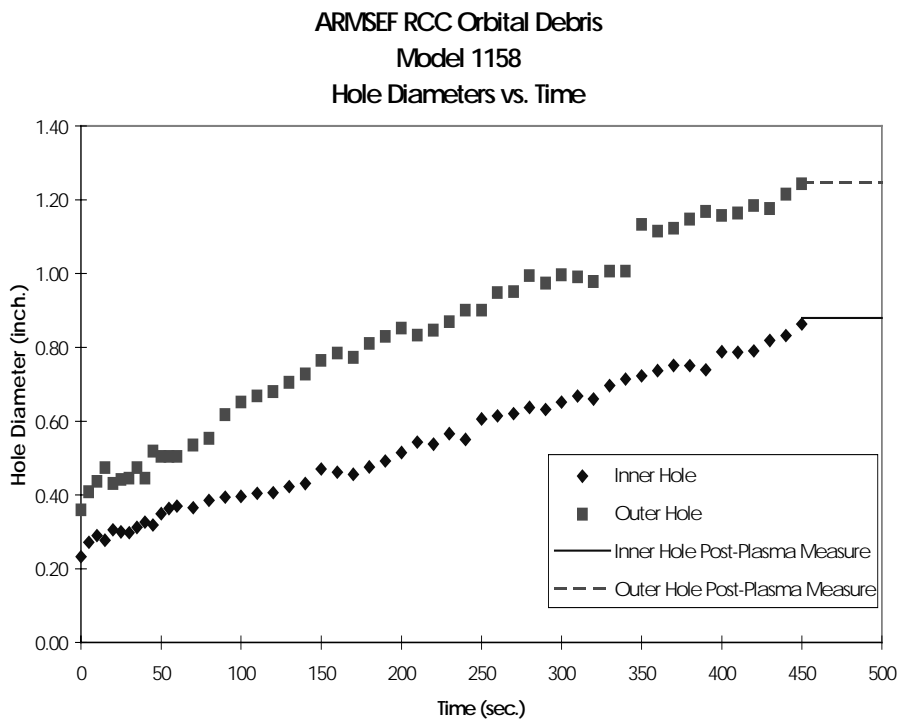**Figure A-1. Photo of Model 1142.**
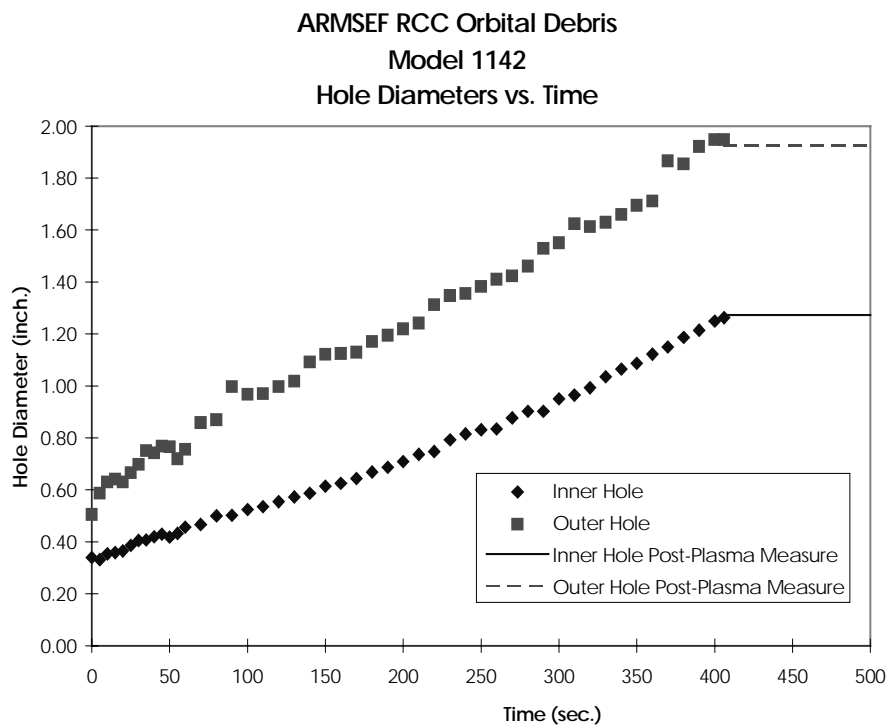
Figure A-2. Graph of hole growth for Model 1142.
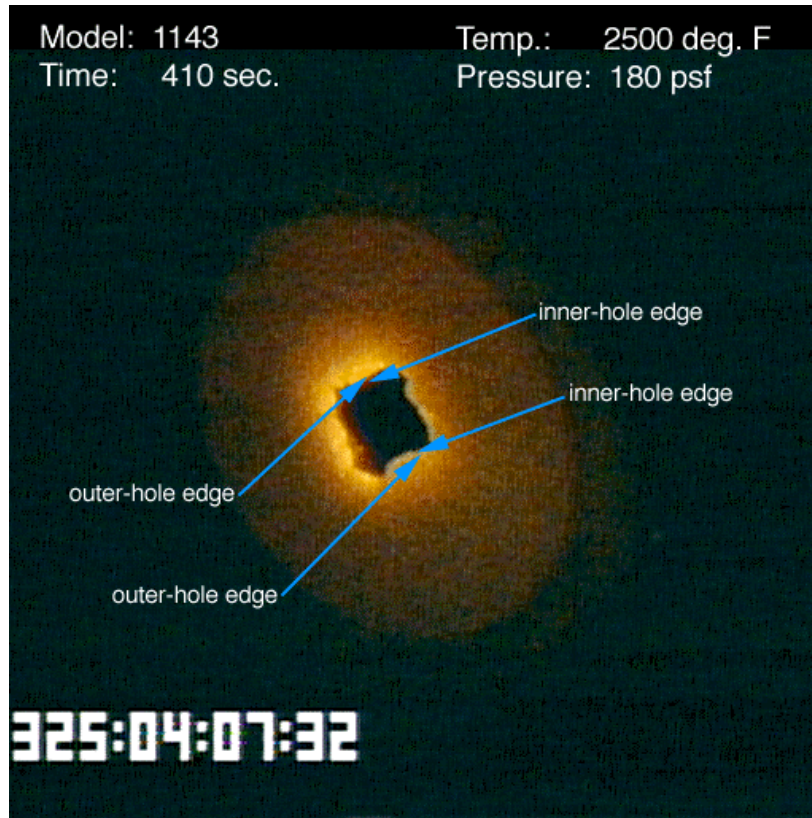
Figure A-3. Photo of Model 1143.
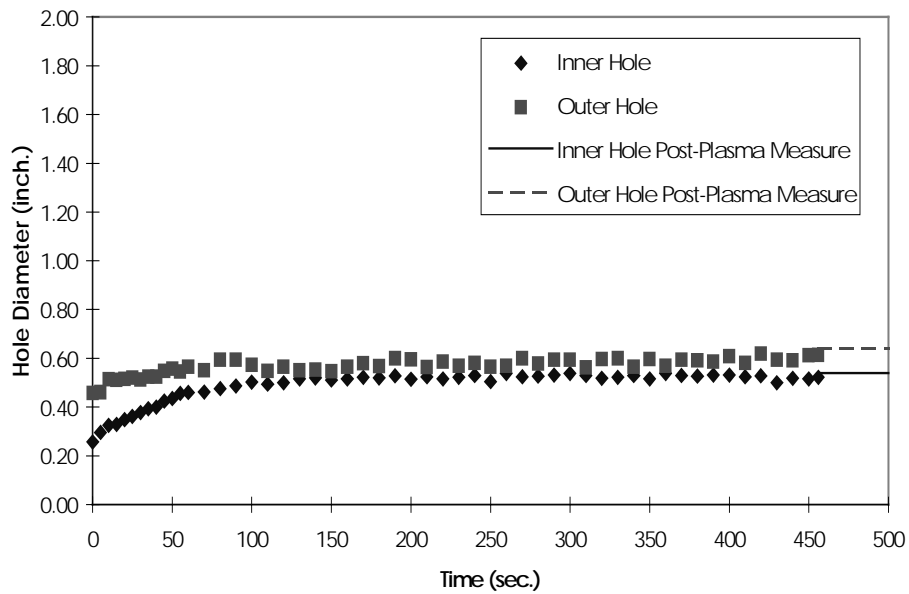
Figure A-4. Graph of hole growth for Model 1143.
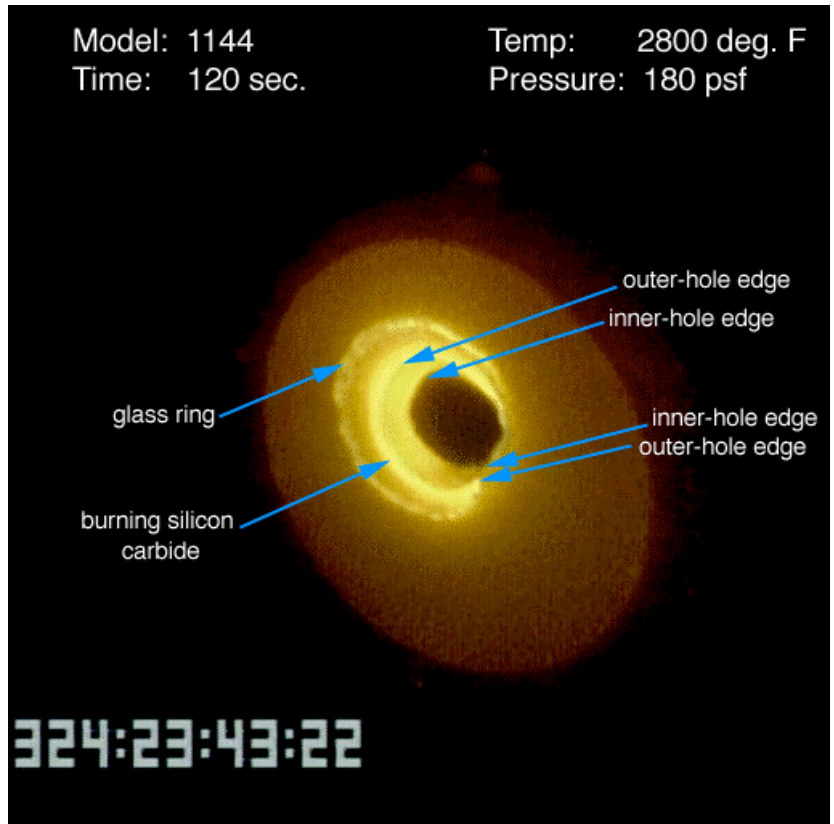
Figure A-5. Photo of Model 1144.
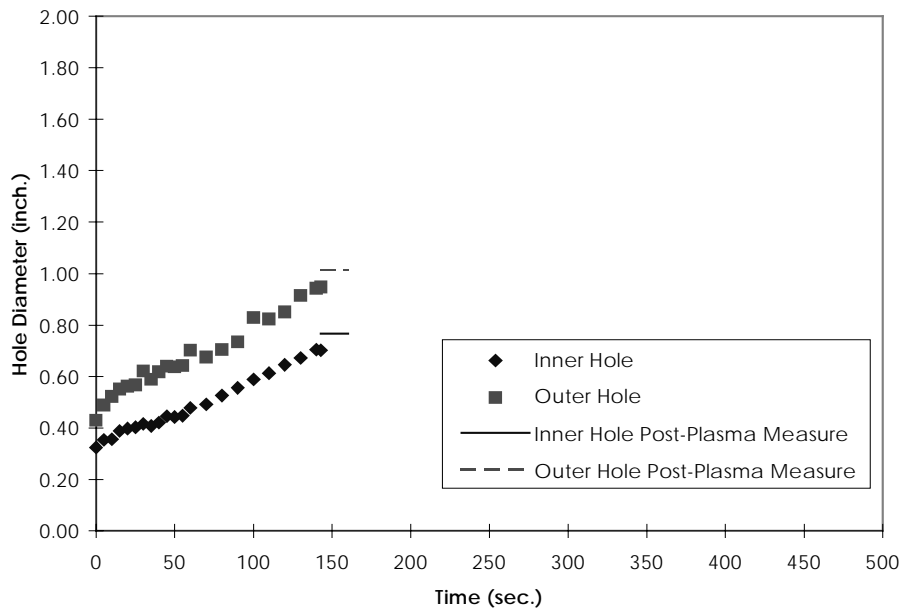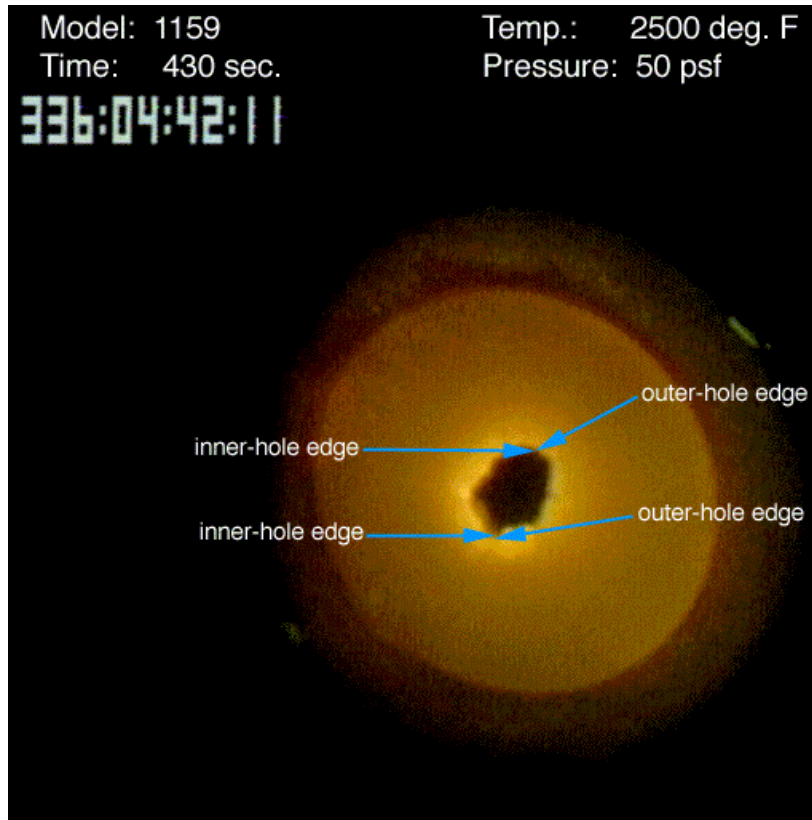

Figure A-6. Graph of hole growth for Model 1144.
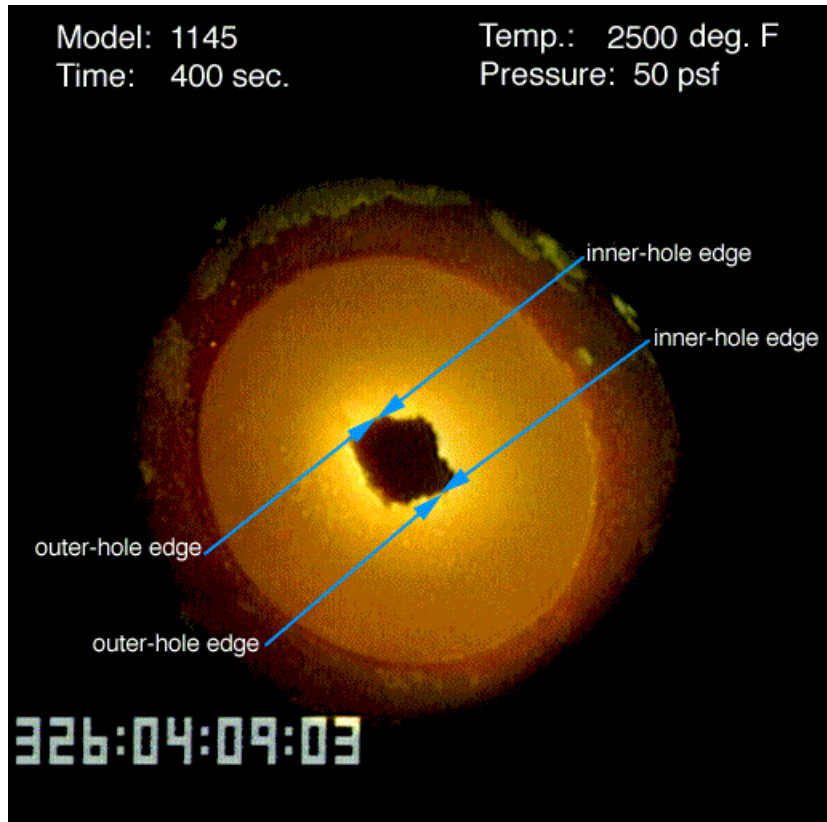
Figure A-7. Photo of Model 1145.
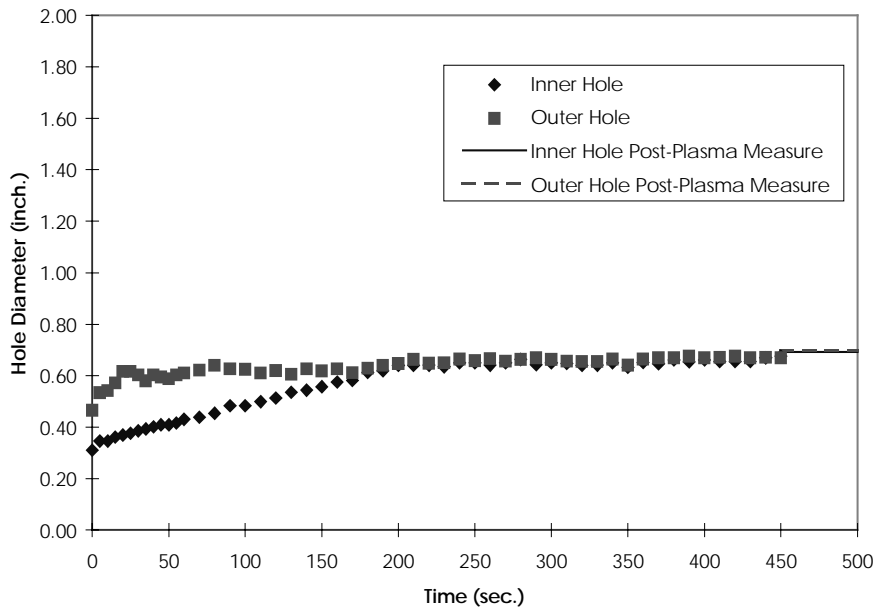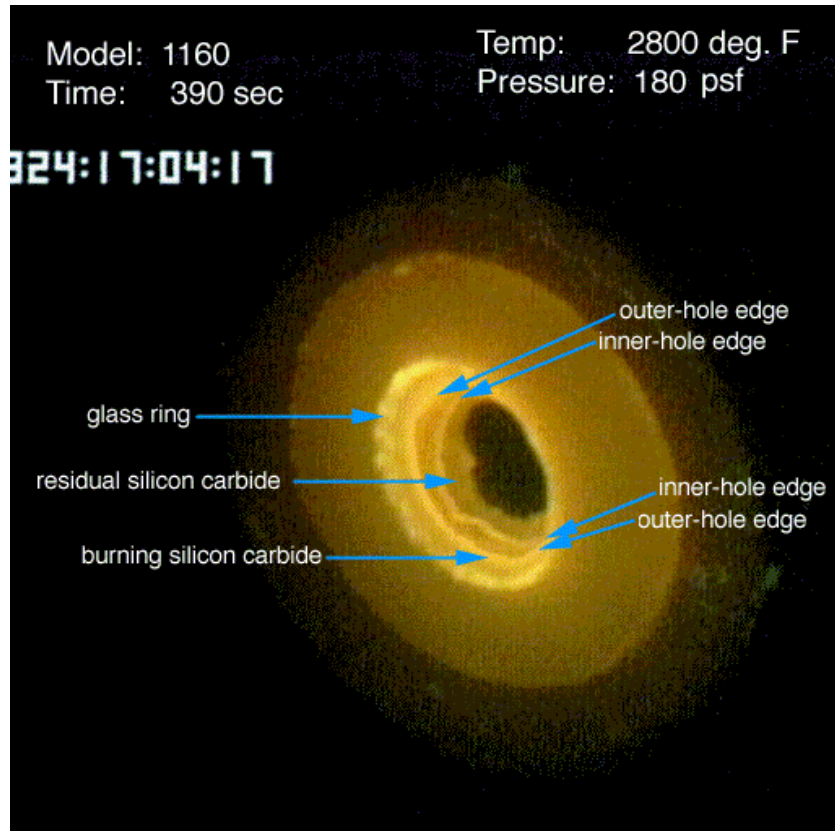

Figure A-8. Graph of hole growth for Model 1145.
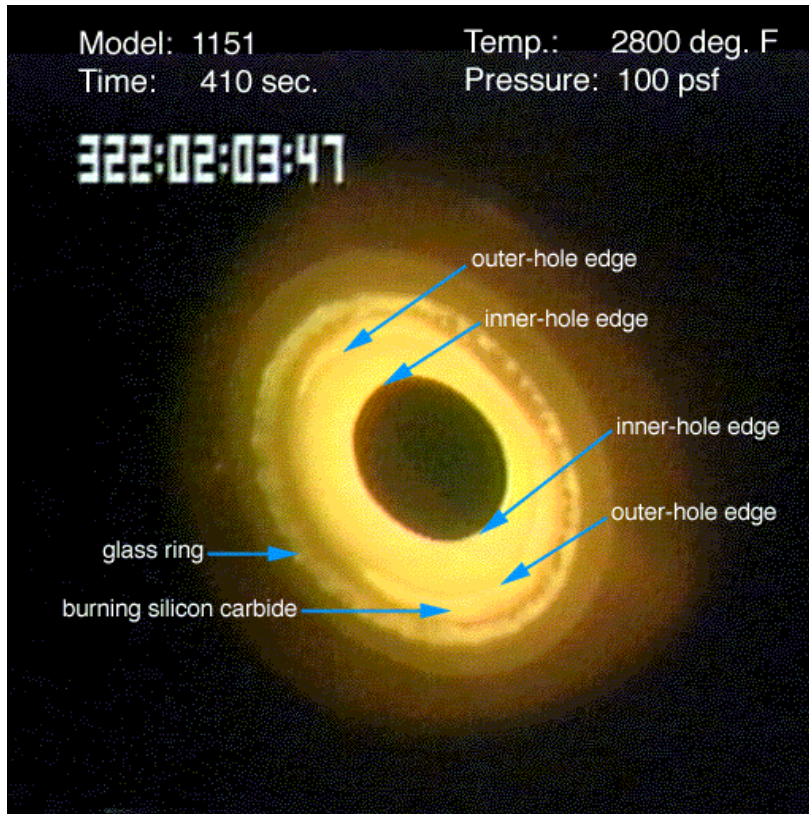
Figure A-9. Photo of Model 1151.
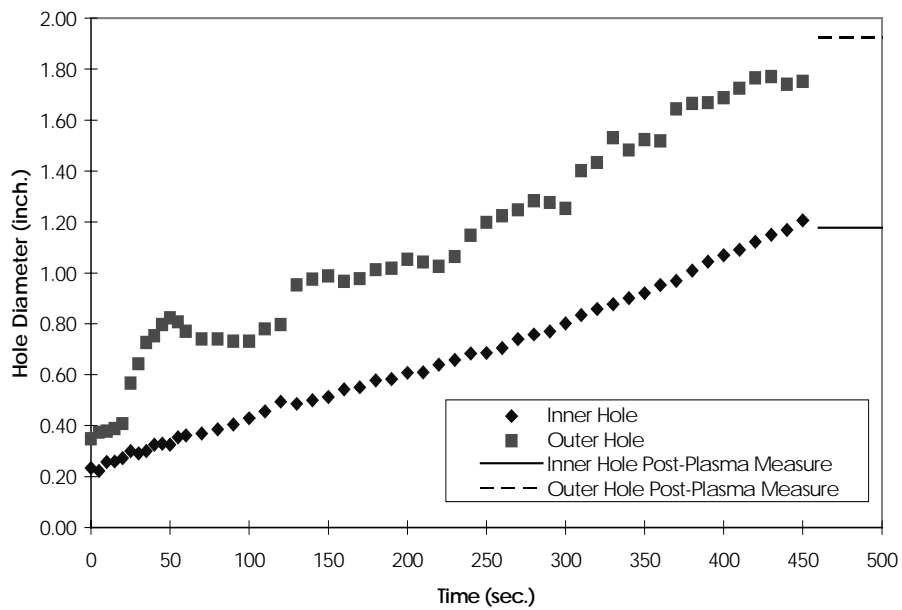
Figure A-10. Graph of hole growth for Model 1151.
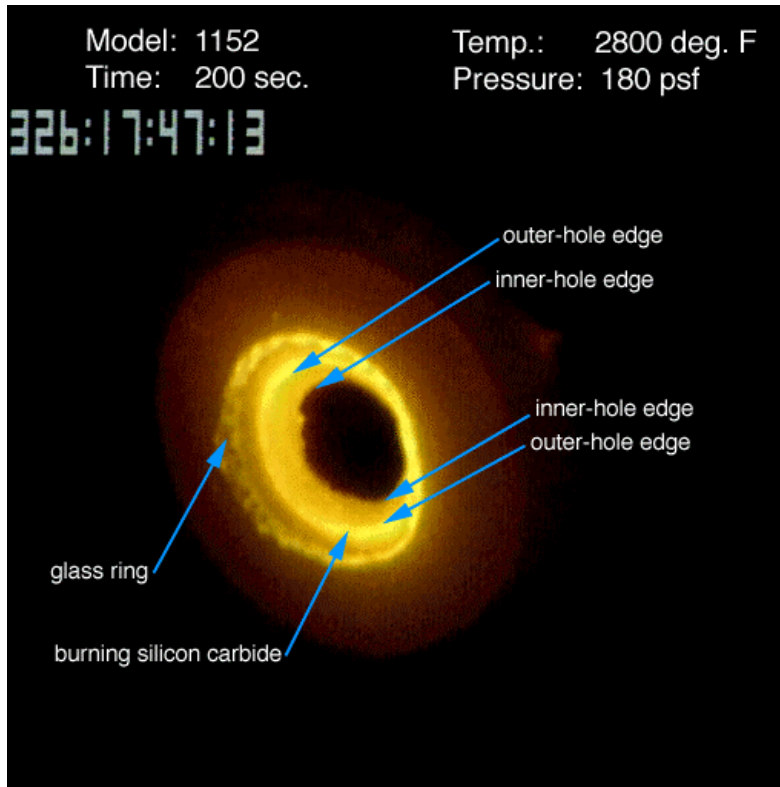
Figure A-11. Photo of Model 1152.

ARMSEF RCC Orbital Debris
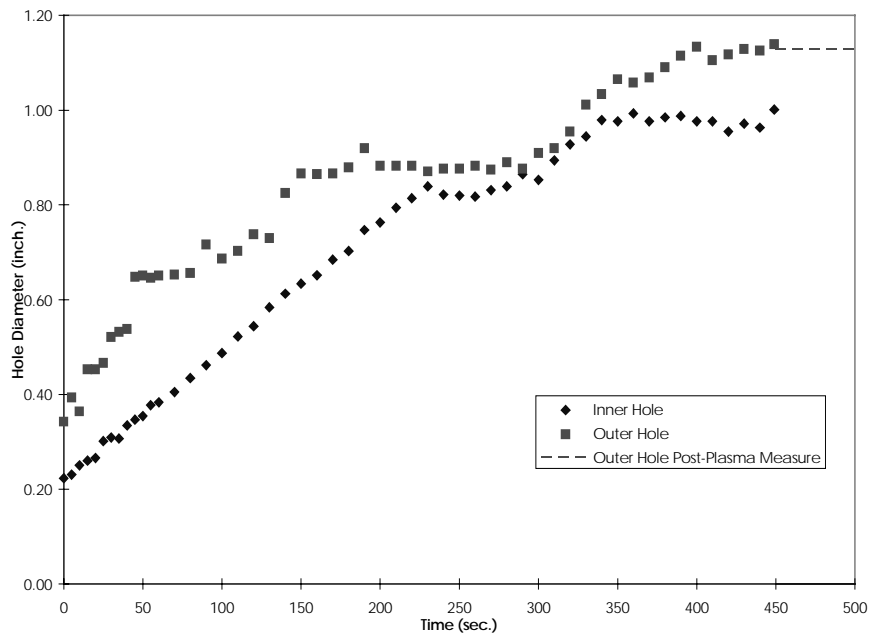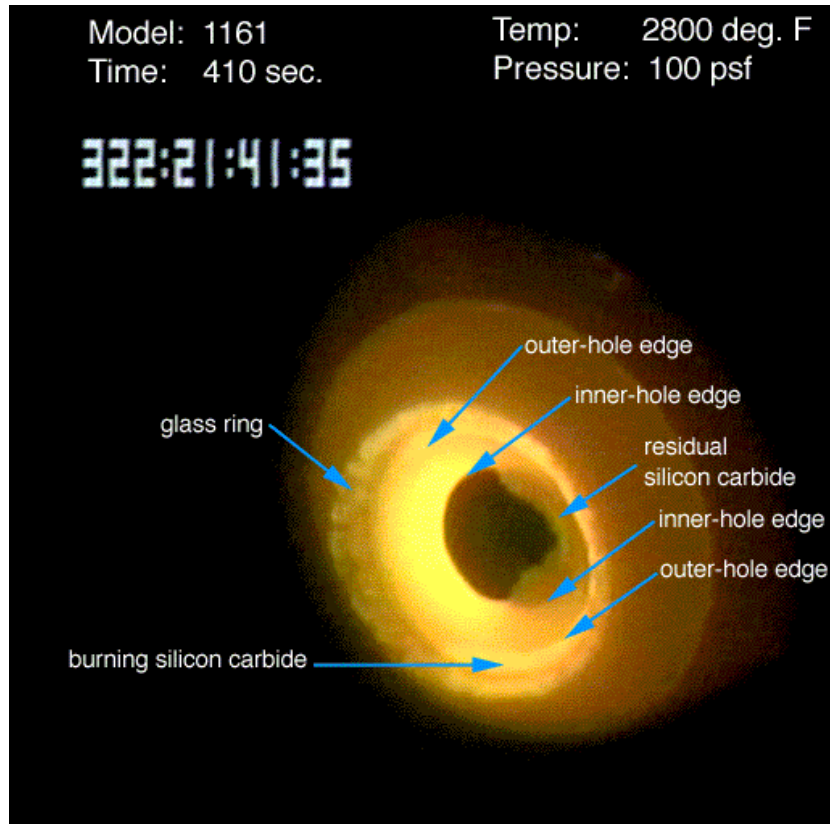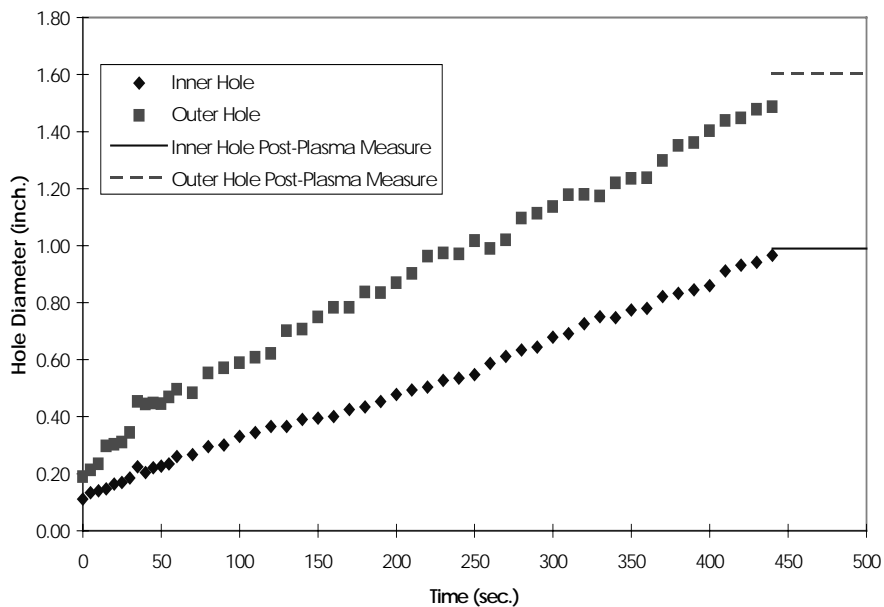Model 1152
Hole Diameters vs. Time
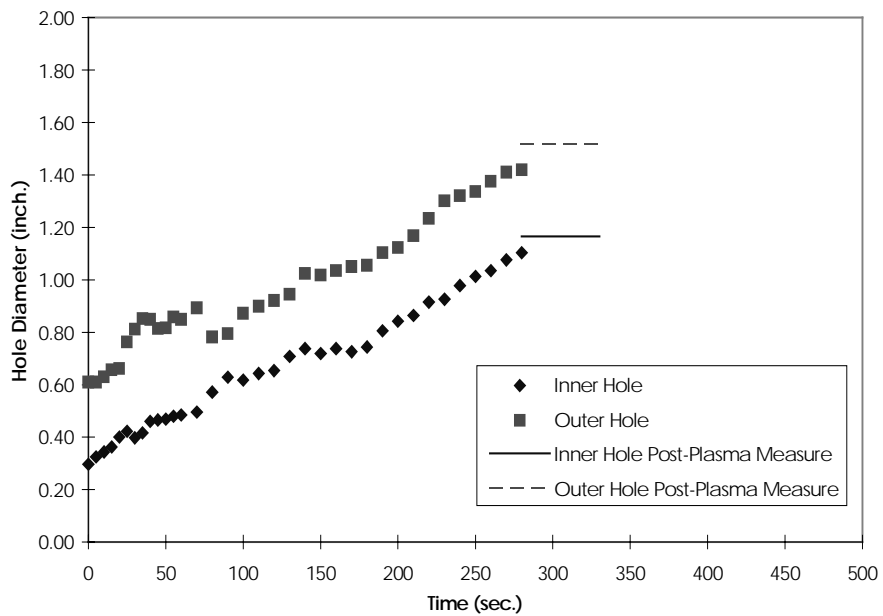
Figure A-12. Graph of hole growth for Model 1152.
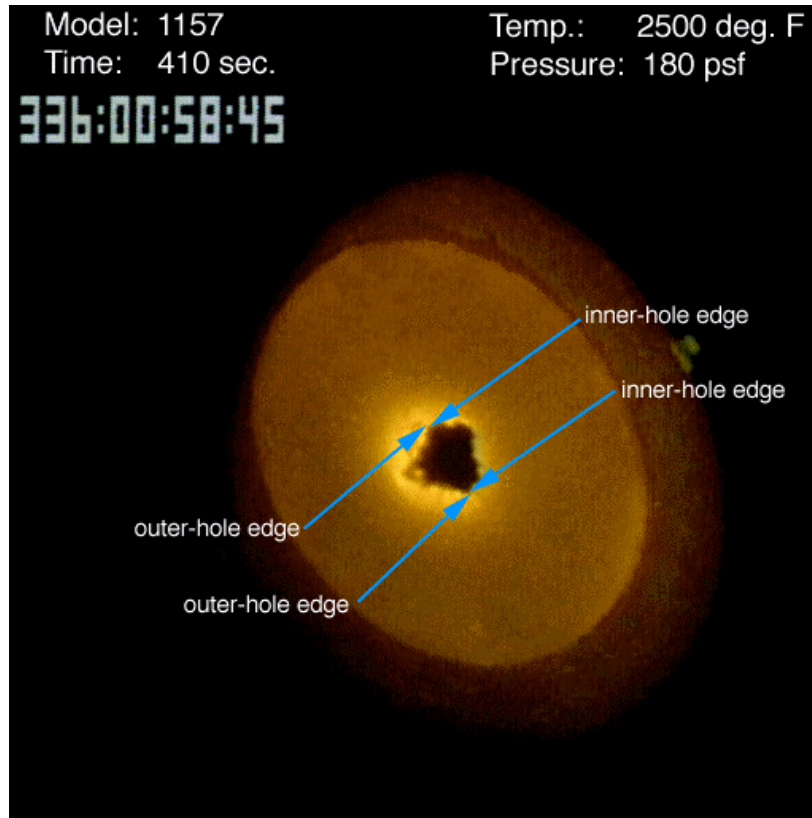
Figure A-13. Photo of Model 1157.

ARMSEF RCC Orbital Debris
Model 1157
Hole Diameters vs. Time
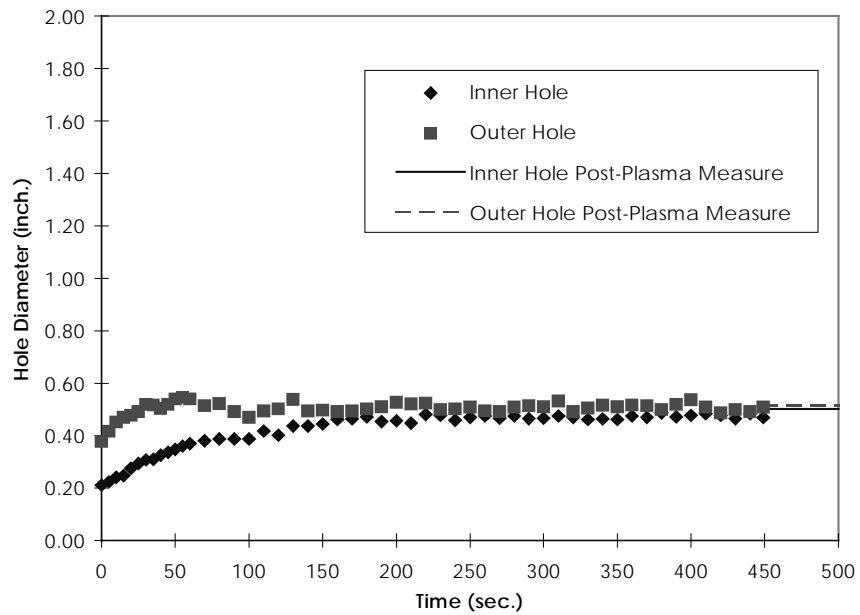
Figure A-14. Graph of hole growth for Model 1157.
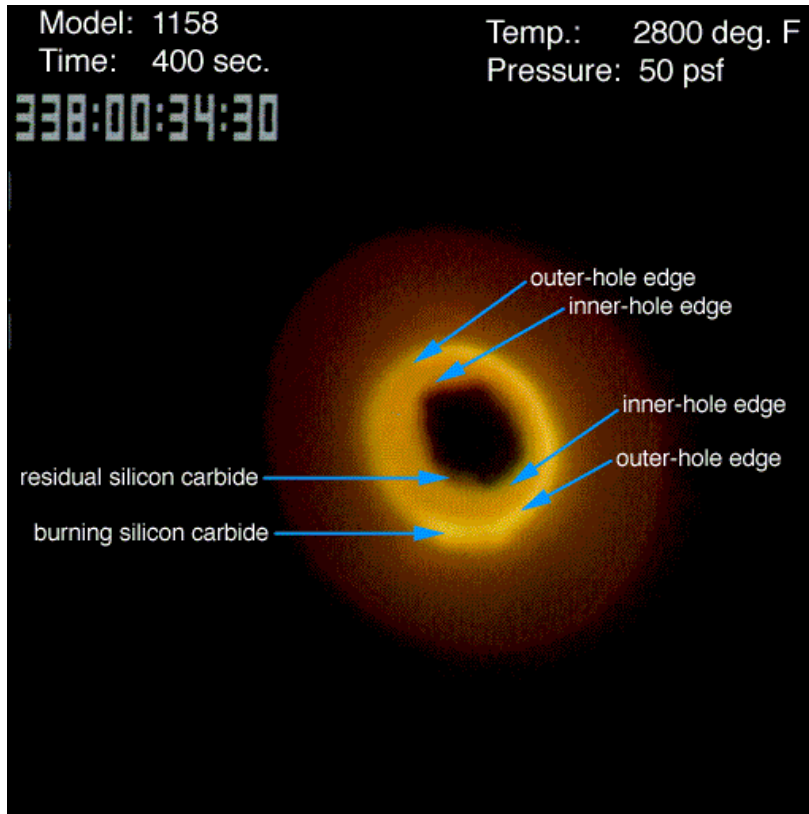
Figure A-15. Photo of Model 1158.

Figure A-16. Graph of hole growth for Model 1158.

Figure A-17. Photo of Model 1159.
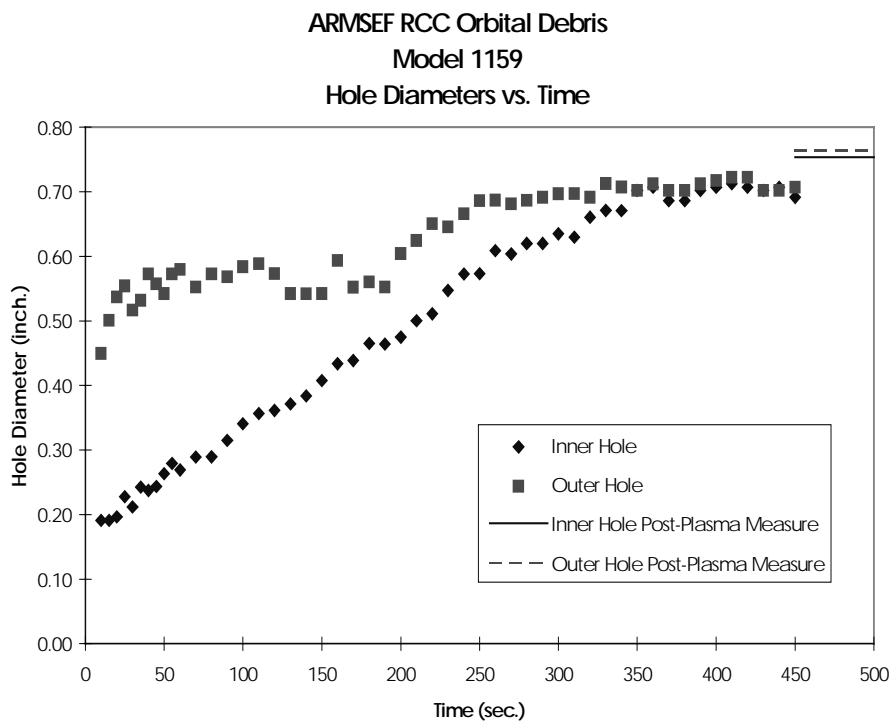
Figure A-18. Graph of hole growth for Model 1159.

34

Figure A-19. Photo of Model 1160.

ARMSEF RCC Orbital Debris
Model 1160
Hole Diameters vs. Time
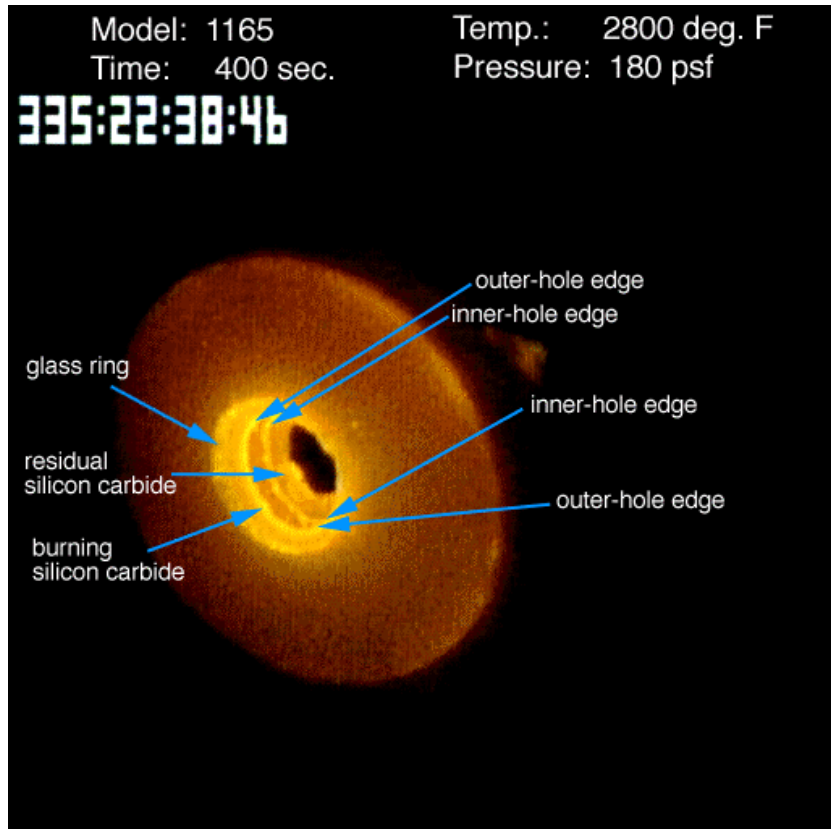

Figure A-20. Graph of hole growth for Model 1160.

Figure A-21. Photo of Model 1161.

Figure A-22. Graph of hole growth for Model 1161.
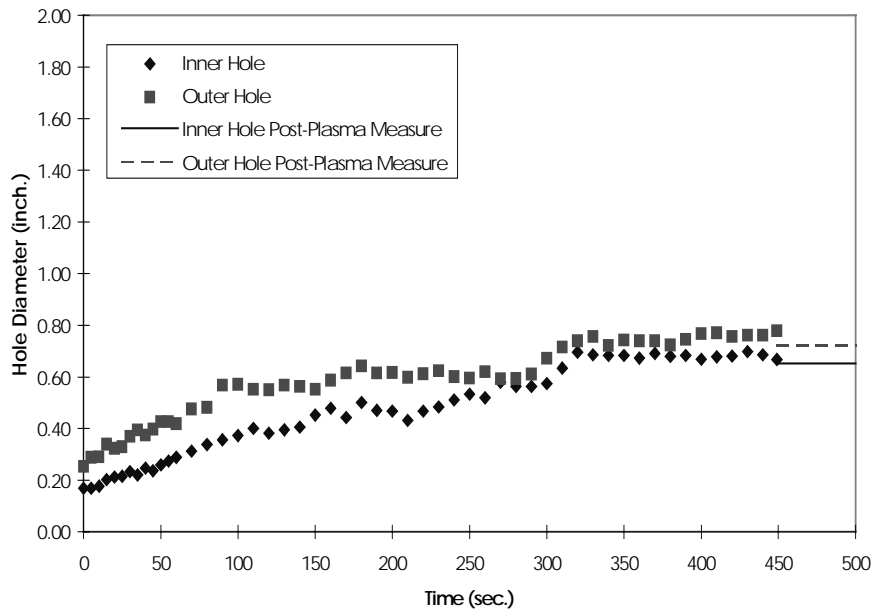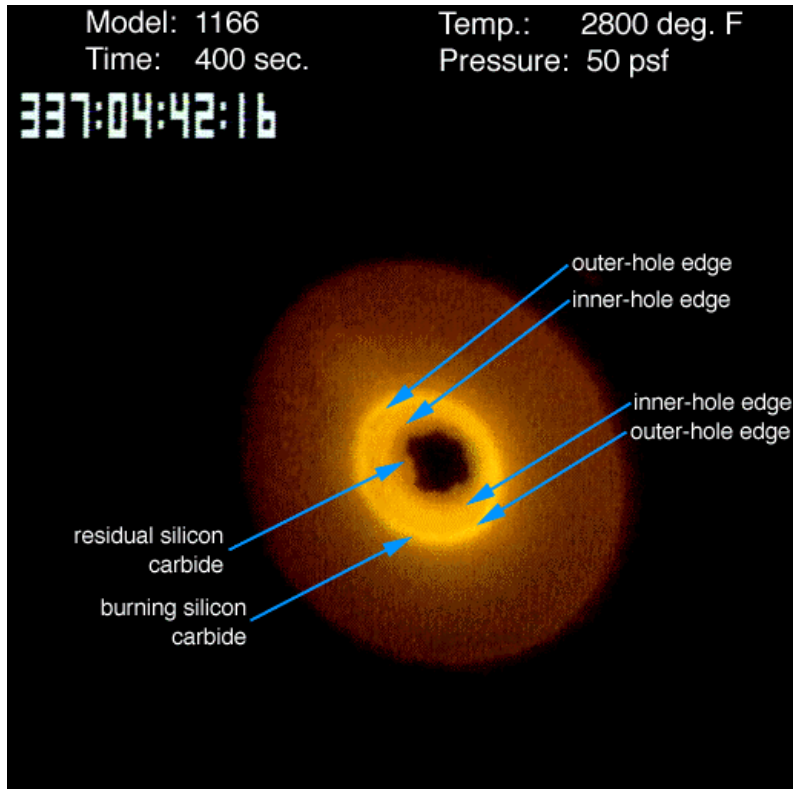
Figure A-23. Photo of Model 1165.

Figure A-24. Graph of hole growth for Model 1165.

Figure A-25. Photo of Model 1166.

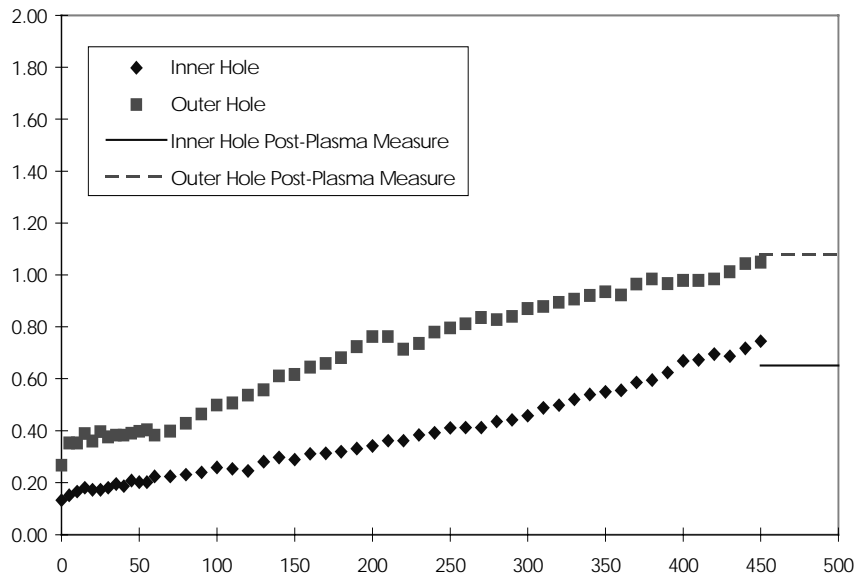ARMSEF RCC Orbital Debris
Model 1166
Hole Diameters vs. Time
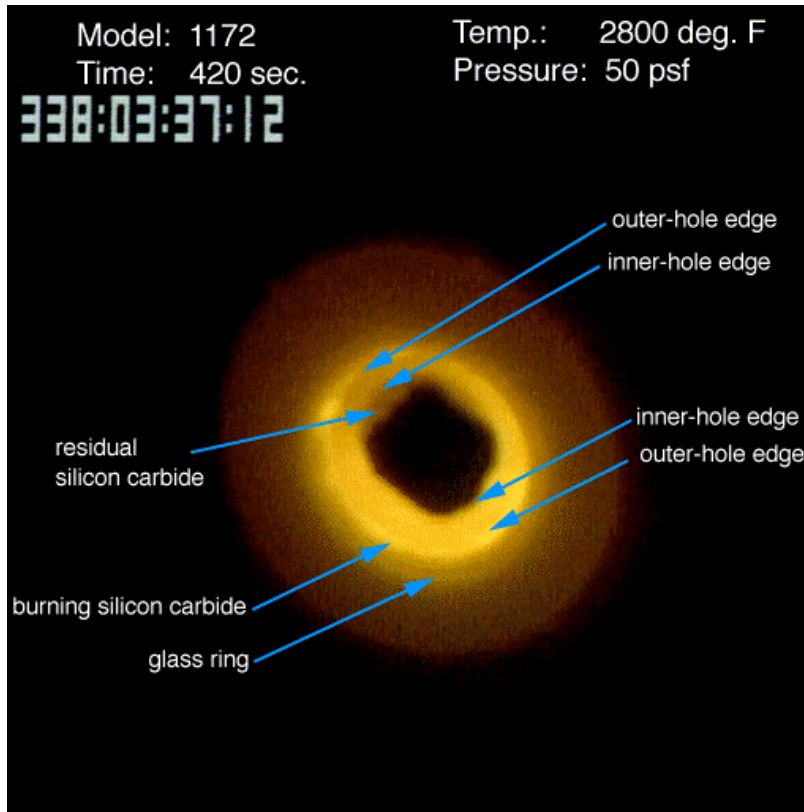

Figure A-26. Graph of hole growth for Model 1166.

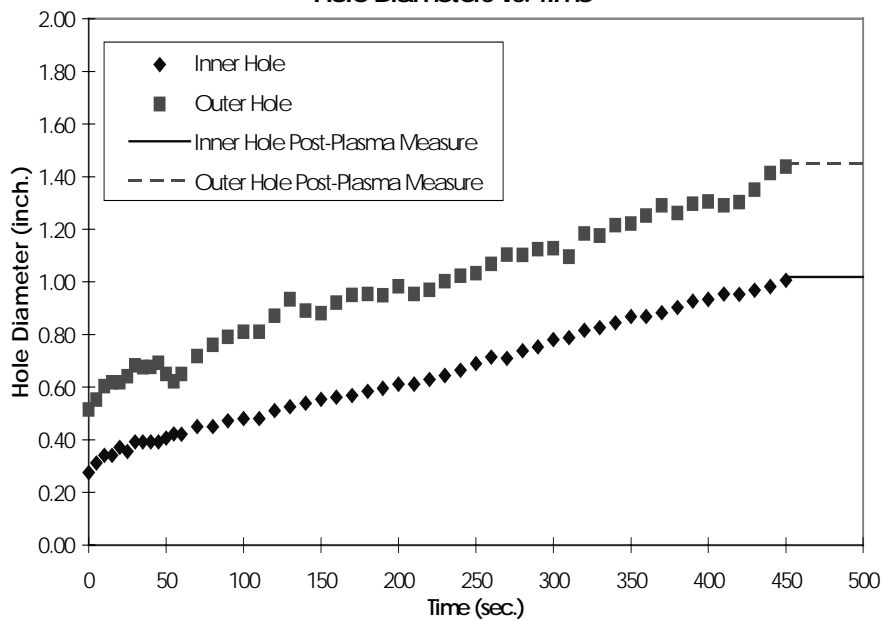**Figure A-27. Photo of Model 1172.**

Figure A-28. Graph of hole growth for Model 1172.

Appendix B

Hole Growth Data

Linear Growth Rate Assumption

Figure B-1 Test Data of An Impacted RCC Hole Growth

Figure B-2 Test Data of An Impacted RCC Hole Growth

Figure B-3 Test Data of An Impacted RCC Hole Growth

Figure B-4 Test Data of An Impacted RCC Hole Growth

43

Figure B-5 Test Data of An Impacted RCC Hole Growth

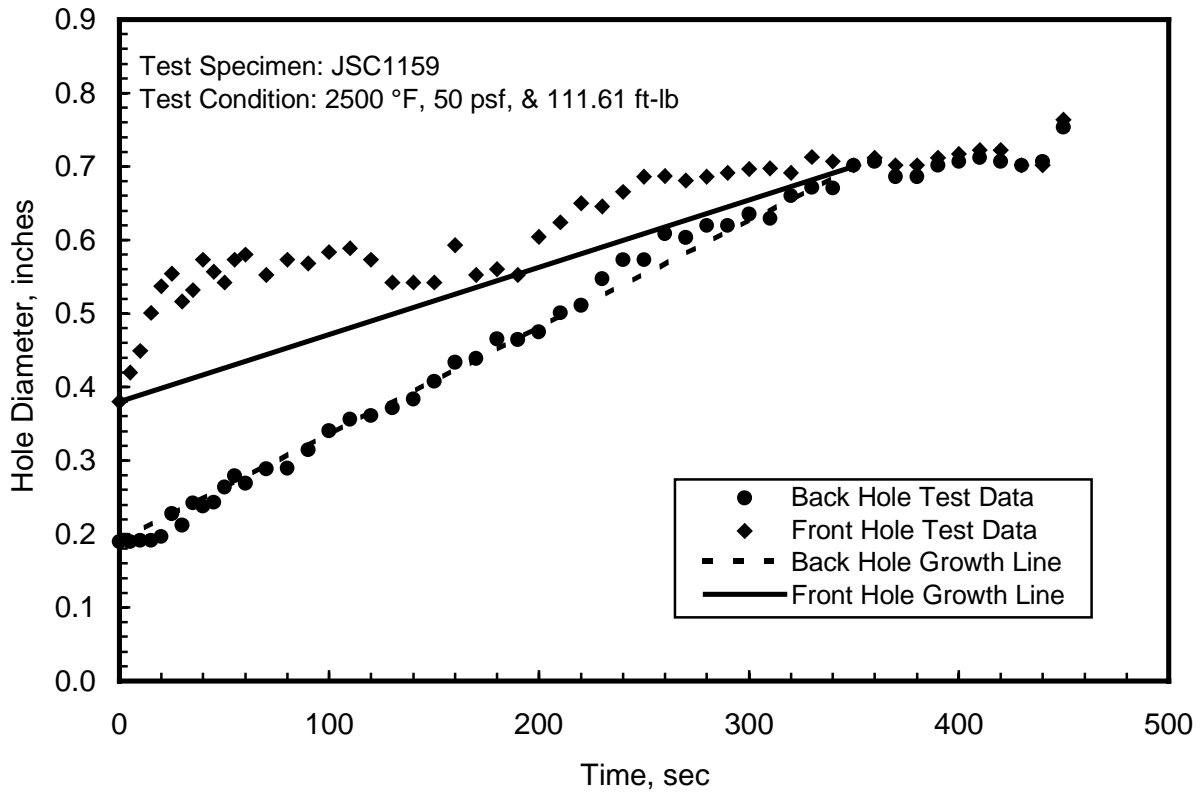Figure B-6 Test Data of An Impacted RCC Hole Growth

44

Figure B-7 Test Data of An Impacted RCC Hole Growth

Figure B-8 Test Data of An Impacted RCC Hole Growth

Figure B-9 Test Data of An Impacted RCC Hole Growth
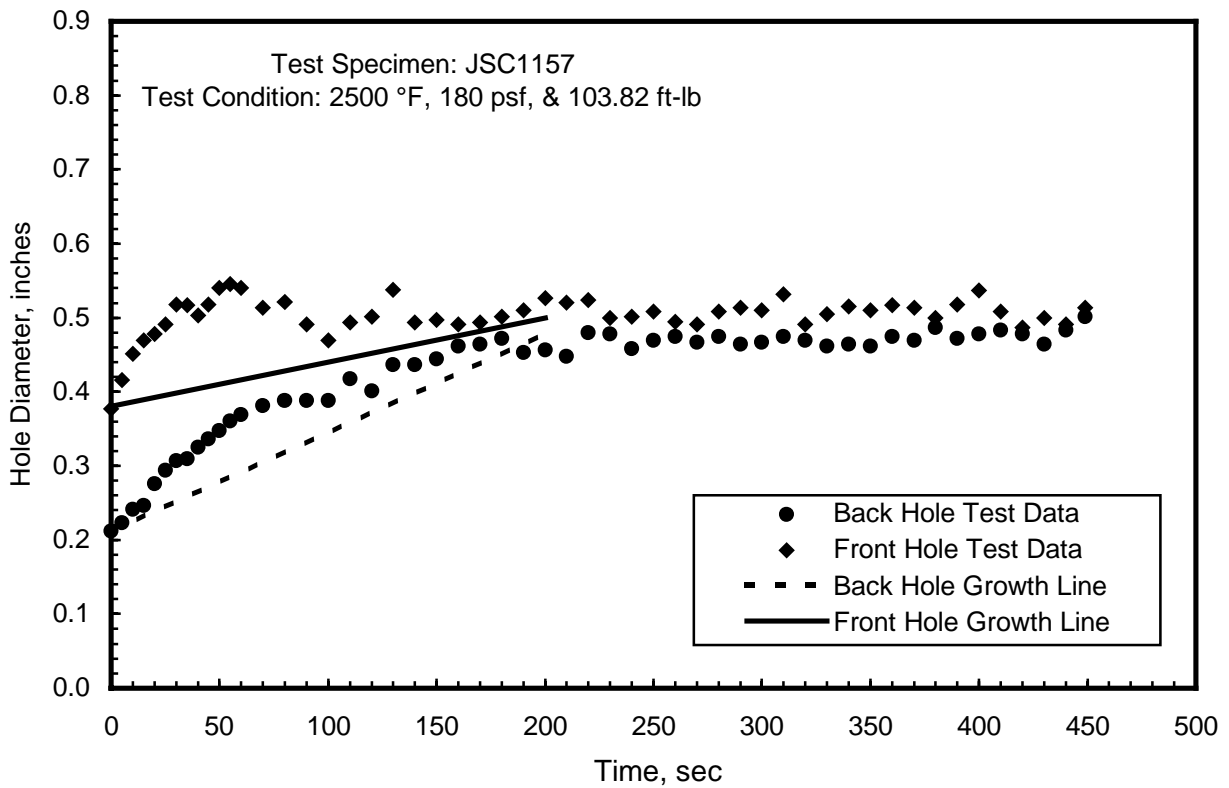

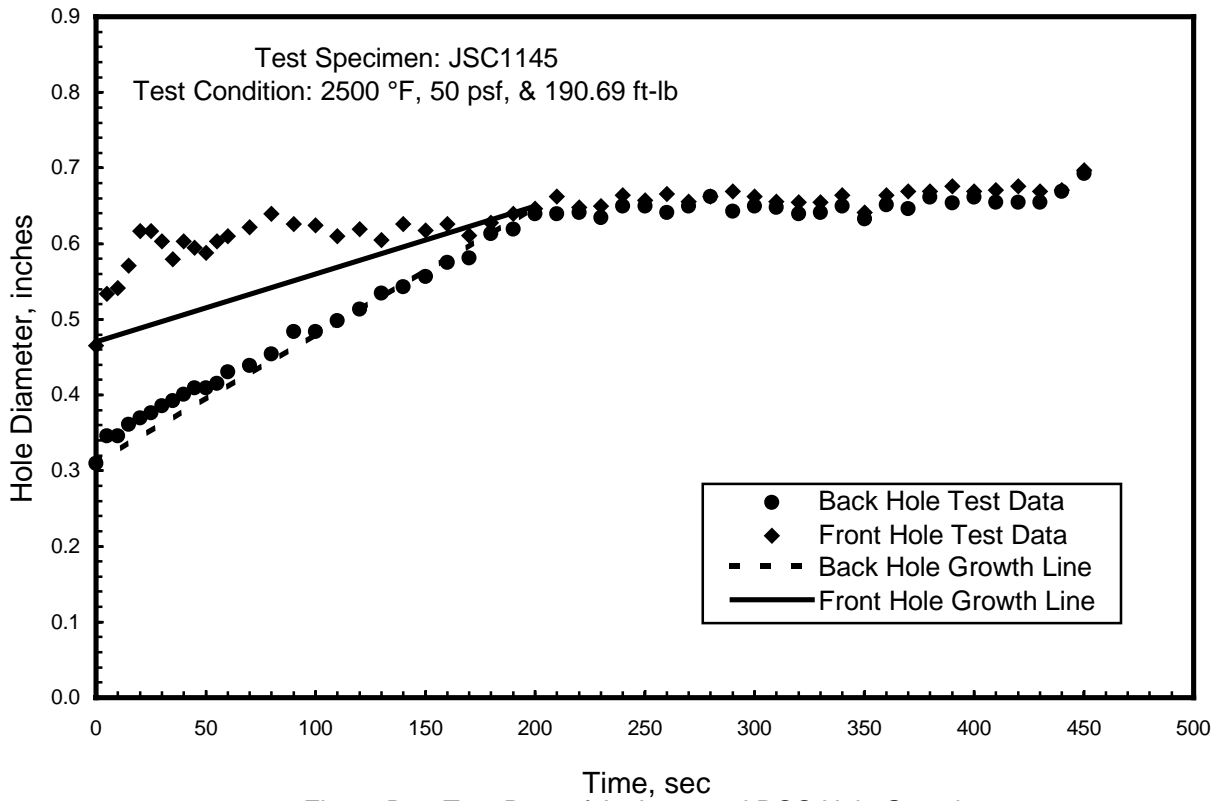Figure B-10 Test Data of An Impacted RCC Hole Growth

Figure B-11 Test Data of An Impacted RCC Hole Growth

Figure B-12 Test Data of An Impacted RCC Hole Growth

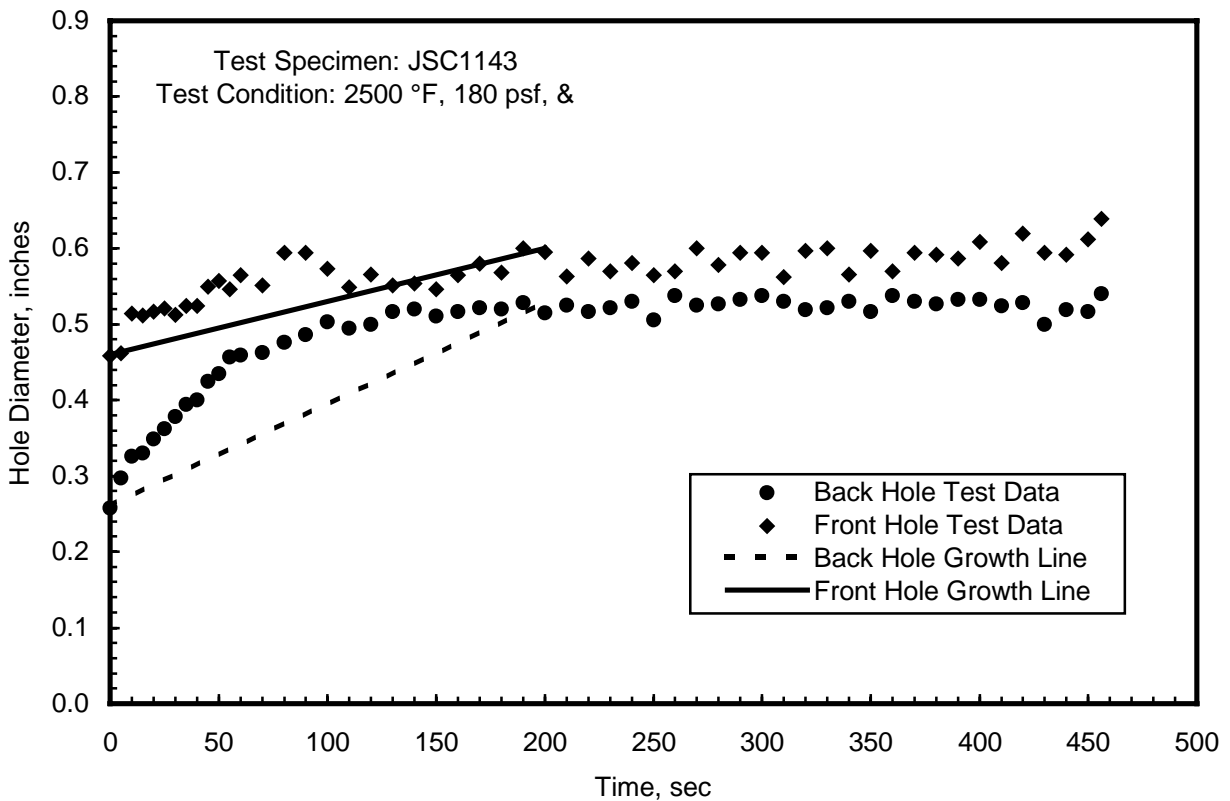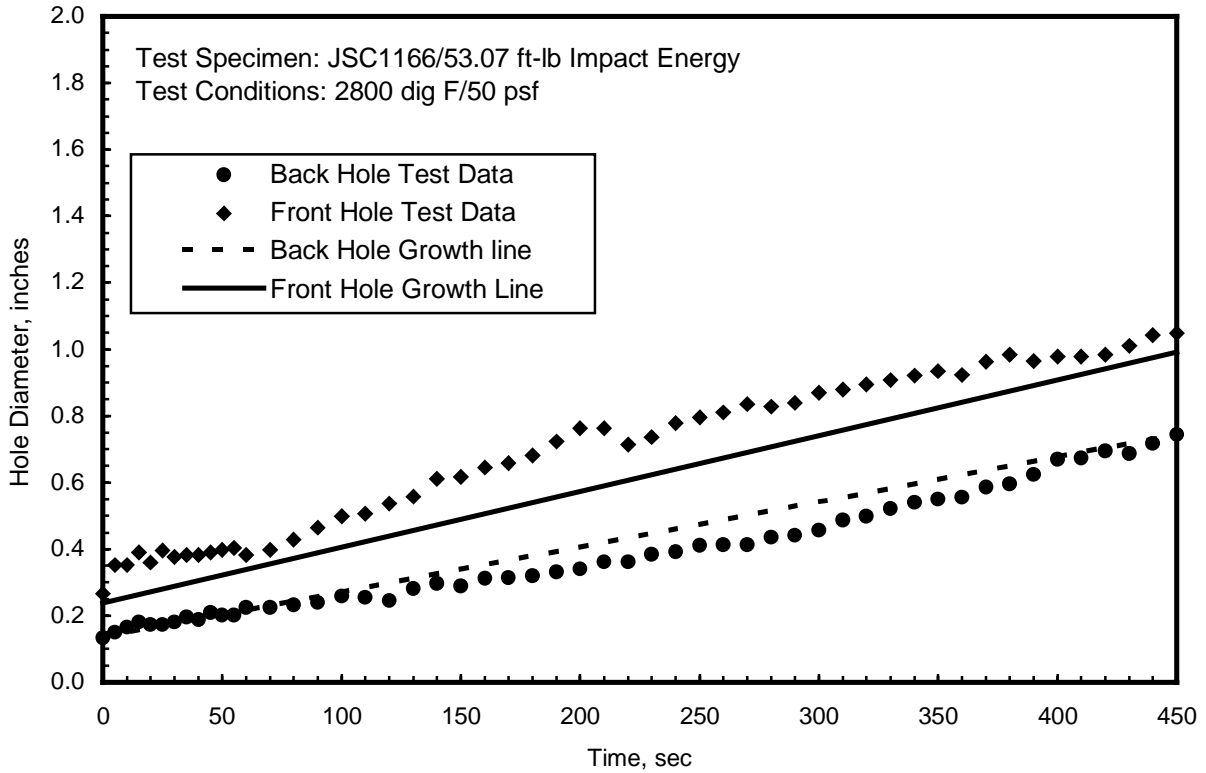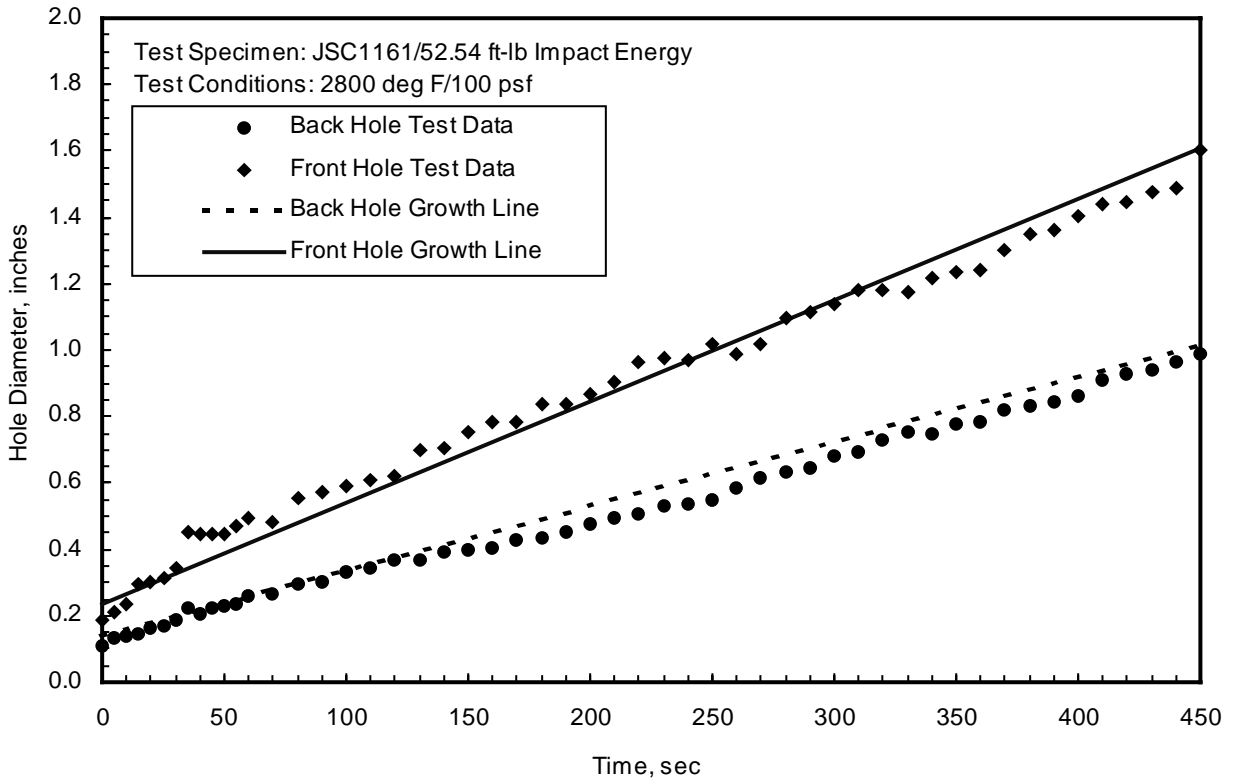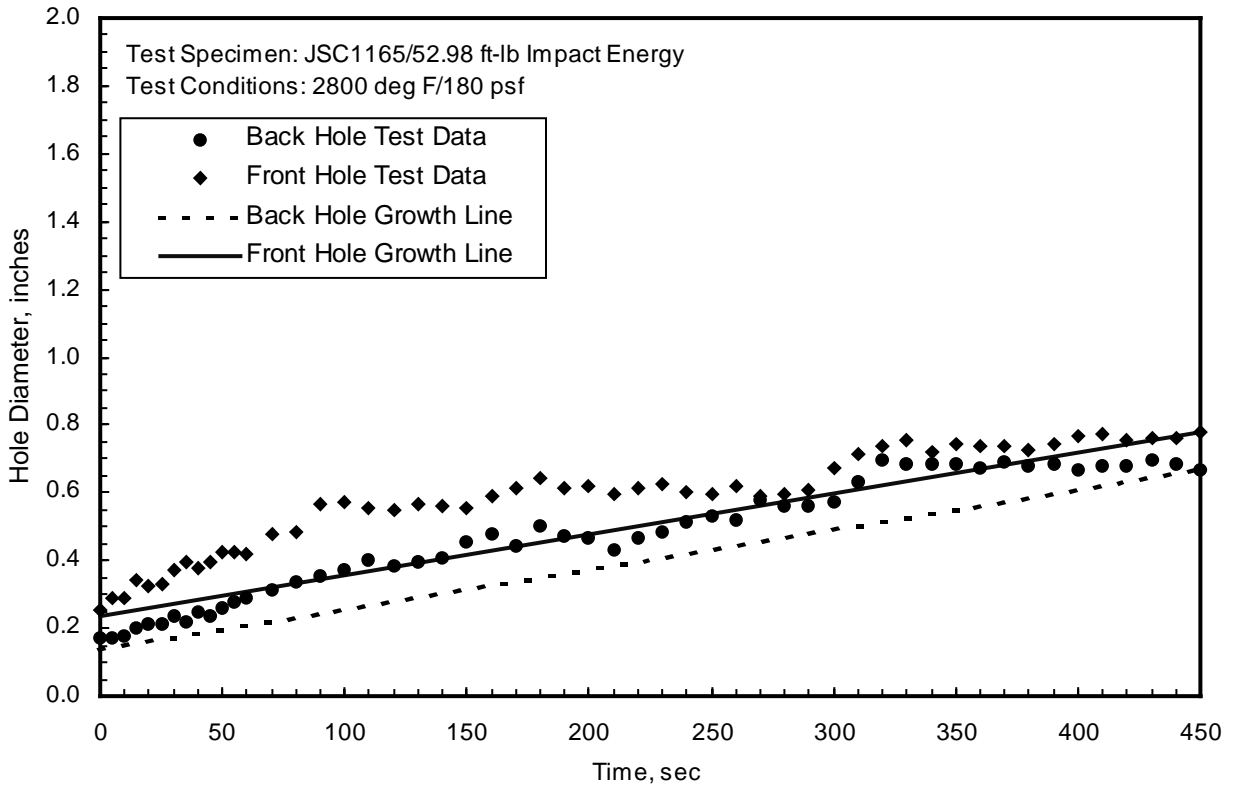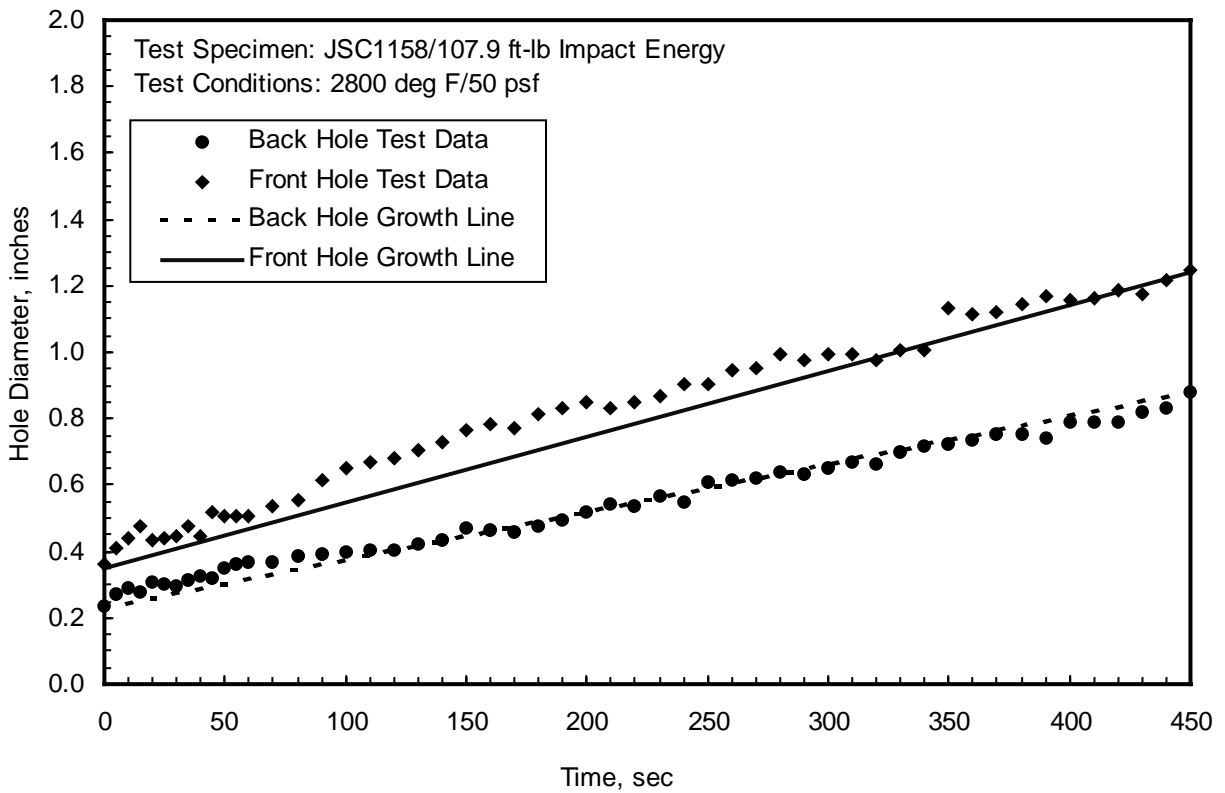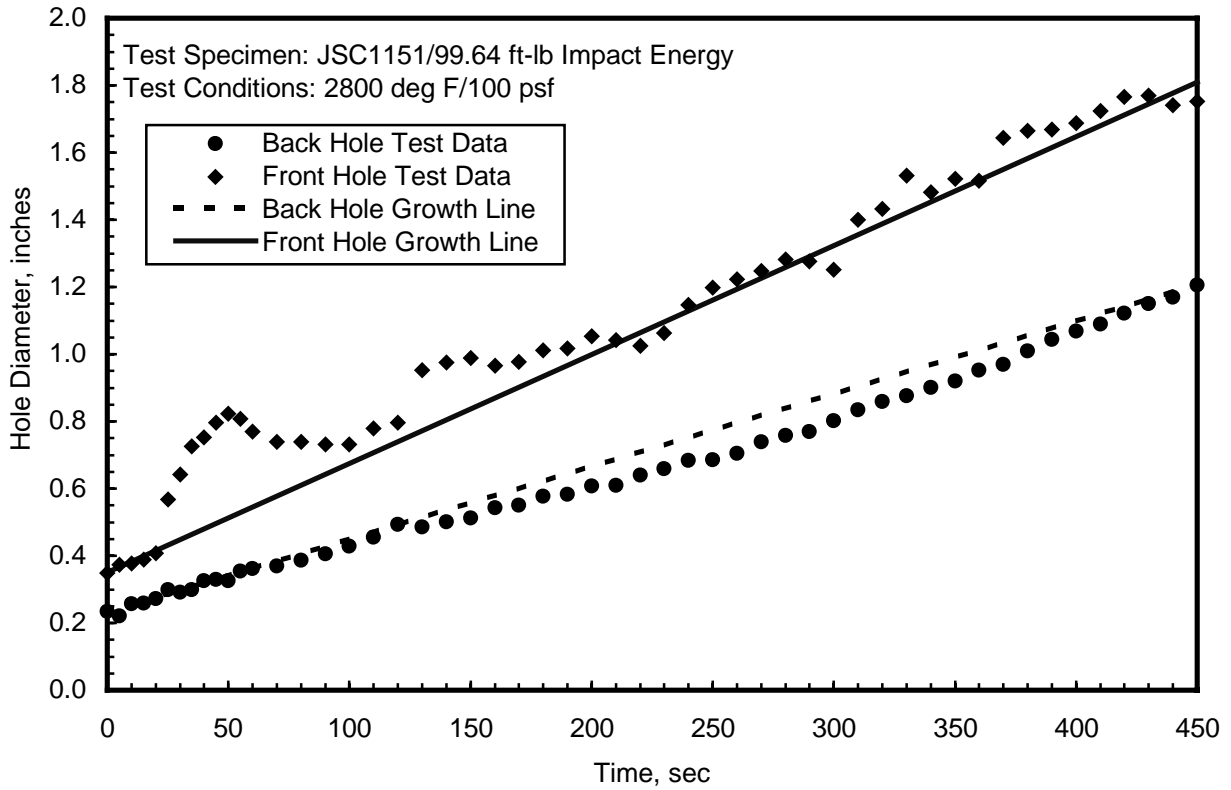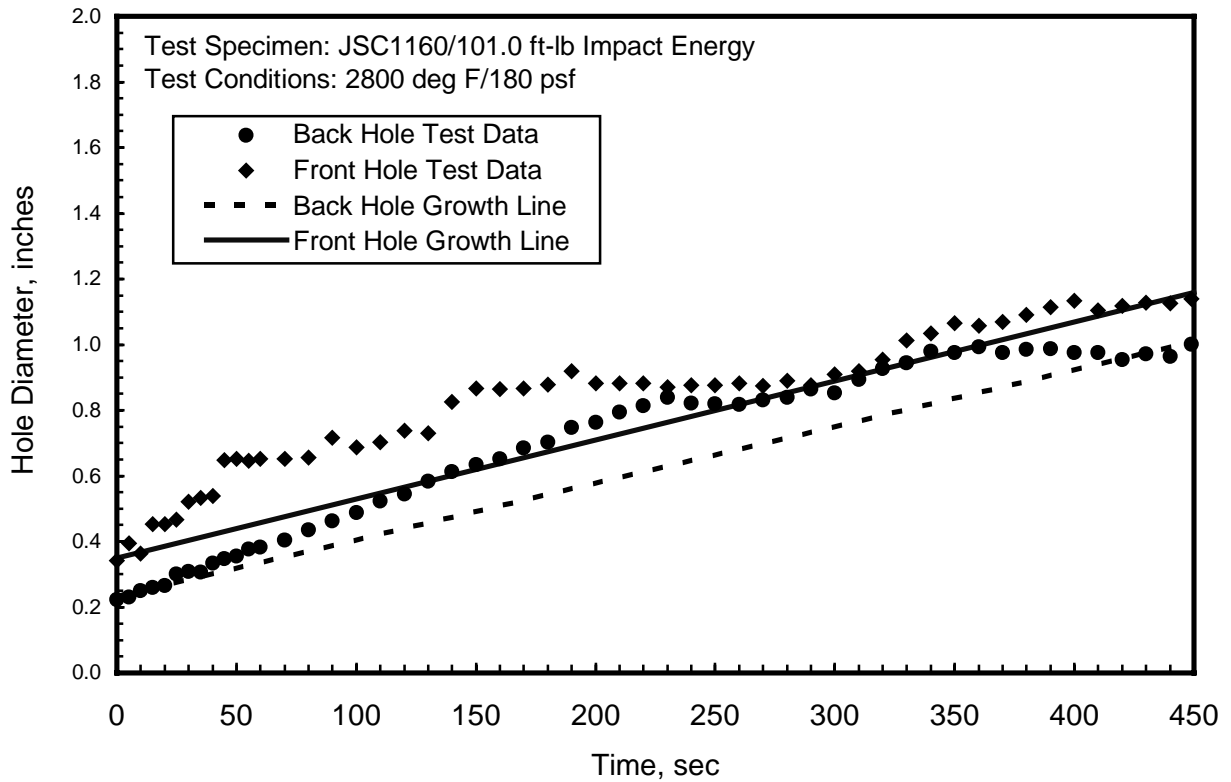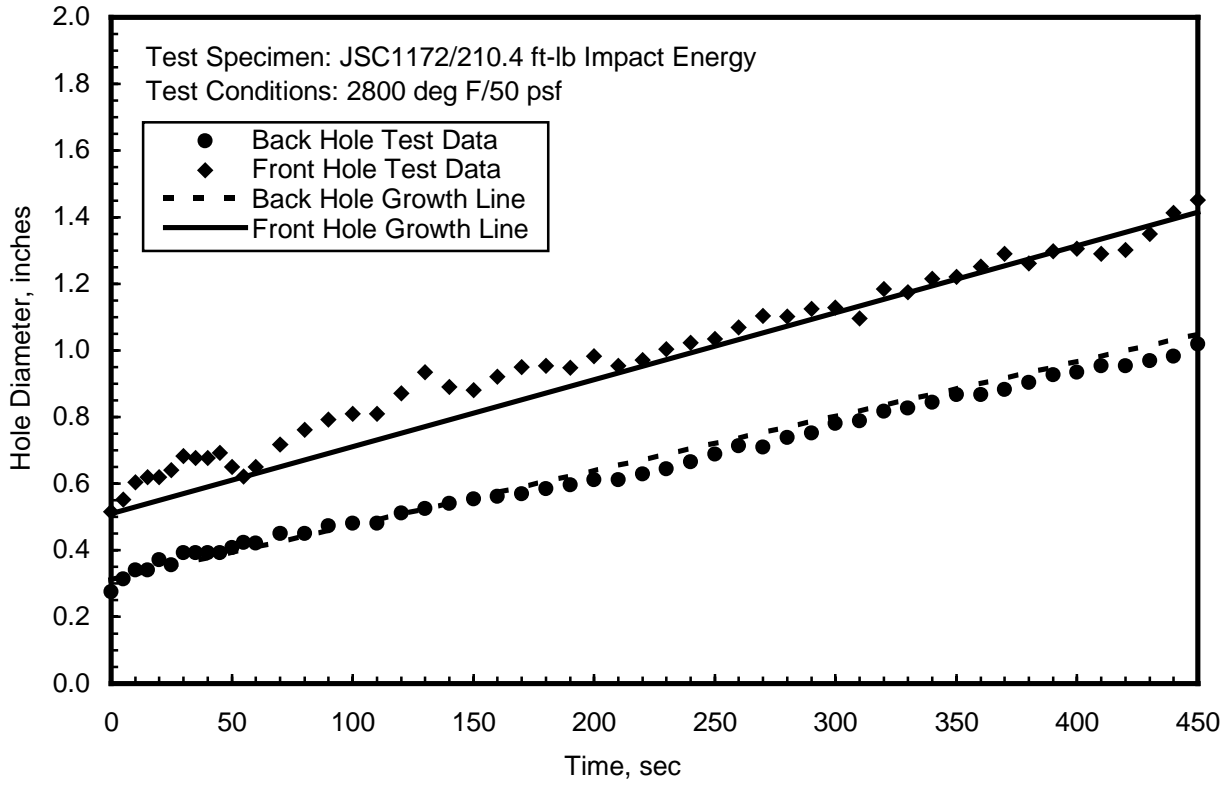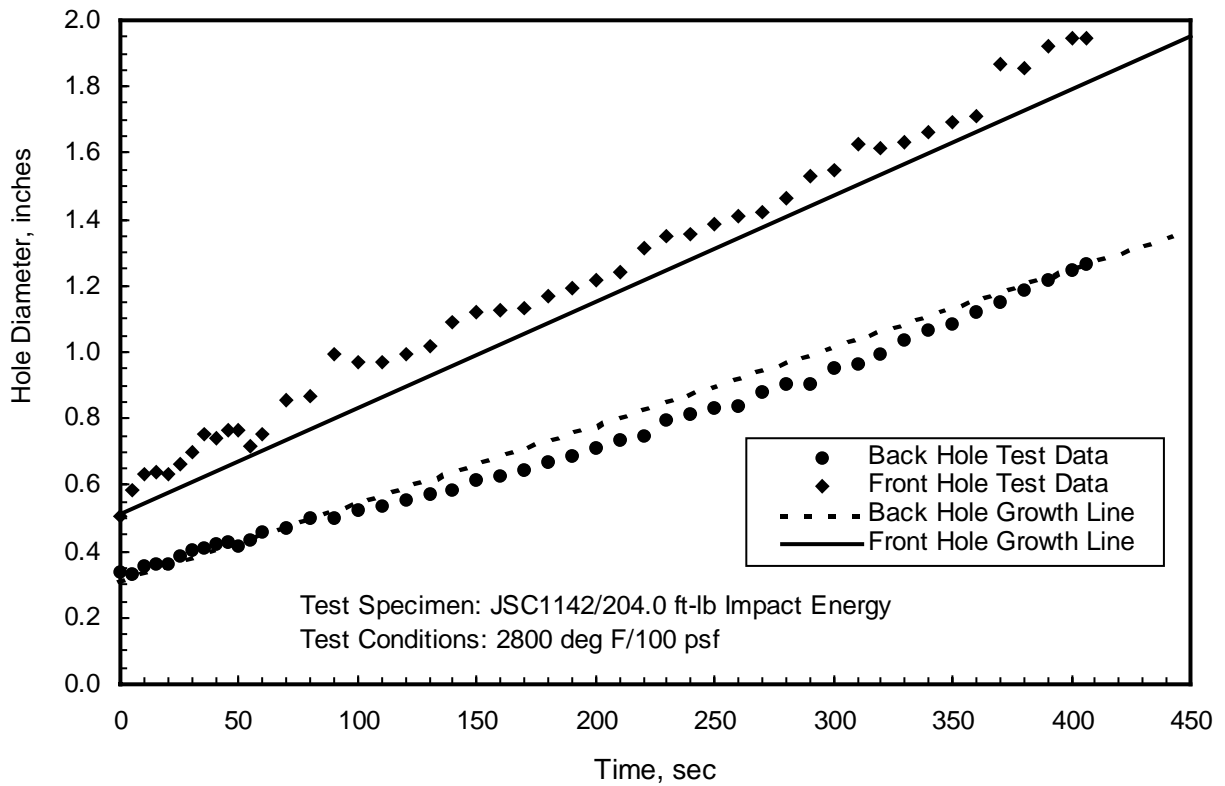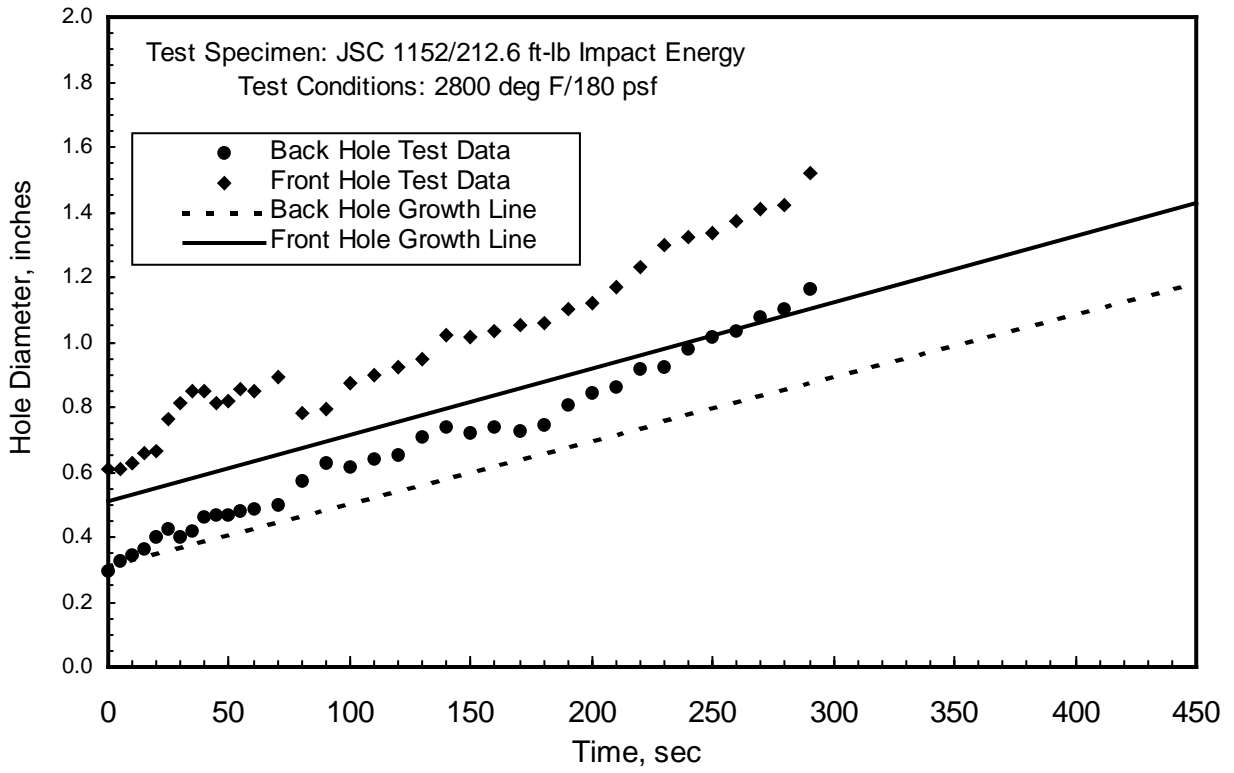Figure B-13 Test Data of An Impacted RCC Hole Growth

Appendix C

Error Analysis

Appendix C - Error Analysis

This error analysis is based on the hole growth or mass loss rate test data. The hole growth test data was obtained by two different methods: pretest and posttest measurements from test specimens and measurement from the test video images. The hole growth measurements made by the JSC IS&AG indicated a minimum uncertainty of 0.01-in.-dia. measurements for the inner hole edge and 0.03 to 0.05 in. for the outer edge diameter. These uncertainties represent an error of approximately 1% to 7% in the final hole diameter as measured from the videotapes. Surface temperature measurement was obtained using calibration models to correlate the surface temperatures measured by laser pyrometer with thermocouples. Test data indicated that the laser pyrometer's readings agreed with the thermocouple within –1.2% to +0.5% of its readings (at temperatures of 2875°F to 3260°F). The presence of an impact damage in the test specimen results in an increased temperature in the local impact area, however, no change in the test conditions were made and all tests were conducted using the calibrated test conditions of a non-impacted test specimen. The comparison of the steady-state readings between laser pyrometer and thermocouples on RCC calibration models can be seen on the data fax from Ron Lewis (NASA/JSC ARMSEF test facility) to I. Norman (Boeing North American) that is attached as the last page of this appendix. Previous analysis of instrumented RCC test specimens indicated that the recorded laser pyrometer surface temperature is within 30°F of the thermal math model predicted surface temperature

Error Analysis for an Impacted RCC Hole Growth at 2500°F Tests

There were only four test data points available for 2500°F test condition, two each at 50 psf and 180 psf pressure environment. Information from pretest and posttest measurements for both test specimens and recorded real-time video images were analyzed to determine the front and back hole growth, and their growth rates. Both methods of obtaining the test data have their advantages. The video image measurements provided very important transient, time-dependent, history information. It showed that at 200 sec after test initiation the front hole growth stopped, and its measurement agreed very well with the measurement of the posttest specimen's front hole diameter. The basic test data for 2500°F test series is shown in table 3.

Measurements from both test specimens and recorded video images were used to perform a regression analysis. The resulting correlation is in terms of a ratio of the RCC substrate mass loss rate with and without an impacted hole. The regression line derived from these data along with ±10% error bands are shown in figure C-1. As can be seen, this provides an excellent correlation of the data and was used in the flight simulation.

Error Analysis for an Impacted RCC Hole Growth at 2800 °F Tests

For the 2800°F test series, ten test specimens were used for nine test points (nine test conditions with three different pressures and three different levels of the impact energy). The last test point at 180 psf pressure and 200 ft-lb of impact energy was tested twice. The first test was aborted at 150 sec after test start; the second was aborted at 14 sec after test start, then retested and aborted again at 290 sec into the test. This was the only test point that did not have a perfect test run.

To eliminate the time dependency of the hole growth rate, test data were translated from hole diameter growth history to hole diameter growth rate assuming an average constant growth rate for each test condition. Because a significant difference appeared between the front and the back hole growth rates, separated correlations were developed for the front and back hole growth. Comparisons of the regression lines with test data along with ±10% error bands are shown in figures C-2 through C-7. These test data are in excellent agreement with the regression lines, except two data points for the front hole growth rate (figure C-4) and one point for the back hole growth rate are out of 10% error band (figure C-7).

Error Analysis for Flight Simulation Application

The temperature range of the test data from this hypervelocity impacted RCC hole growth test program was limited: two temperature points, 2500°F and 2800°F. The flight simulation was based on previous test data correlations (reference 7) and the correlations developed from this current test program.

The following assumptions were made:

1. The 2500°F test series had two different pressures and two different levels of impact energy. Therefore, the substrate mass loss rate correlation for 2500°F condition was developed as a linear function of pressure. No significant effect of impact energy on the substrate mass loss appeared in the 2500°F test data; therefore, it was not included in the 2500°F correlation.

2. Because there is no impact/thermal test data available for temperature between above 2500°F and below 2800°F, an assumption was made that the RCC substrate mass loss correlation developed from 2500°F test data of the current test program, in conjunction with the bare RCC mass loss correlations developed from the previous RCC test programs, will hold for that temperature range (reference 7).

3. Because of the limited test data and to simplify the correlation formulations, it was assumed that the RCC mass loss rate was constant rate with respect to time. The correlations developed in this program were

   - For 2500°F condition, the mass loss rate was an average over 200 sec test time.

   - For 2800°F condition, the mass loss rate was an average over 450 sec test time.

Flight simulations made using the above assumptions and correlations provide a good engineering prediction (±10%) of expected hole growth knowing the initial impact damage (i.e., penetration diameter). Spatial hole growth for a typical Space Station return entry, with an initial hole penetration of 0.025, is shown in figure 24. The correlations are in good agreement with the limited test data. The error analysis indicates that the correlations can be used with confidence in predicting the growth of impacted holes in RCC for flight conditions.
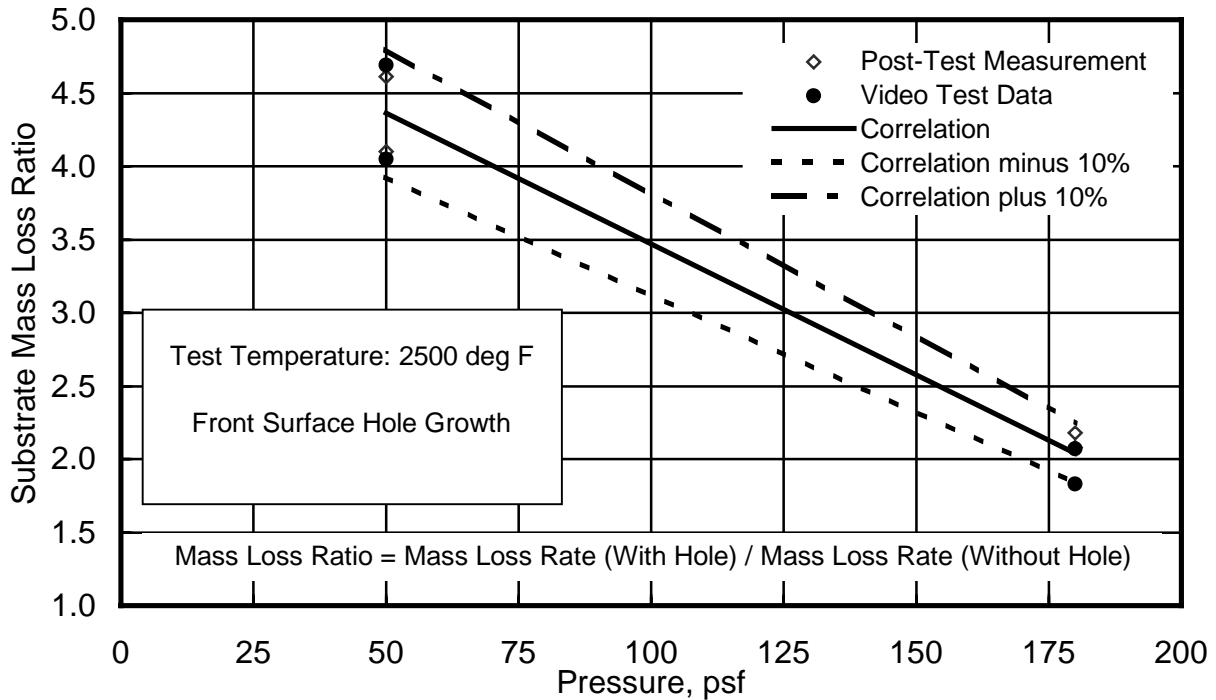

Figure C-1 RCC Substrate Mass Loss Ratio of
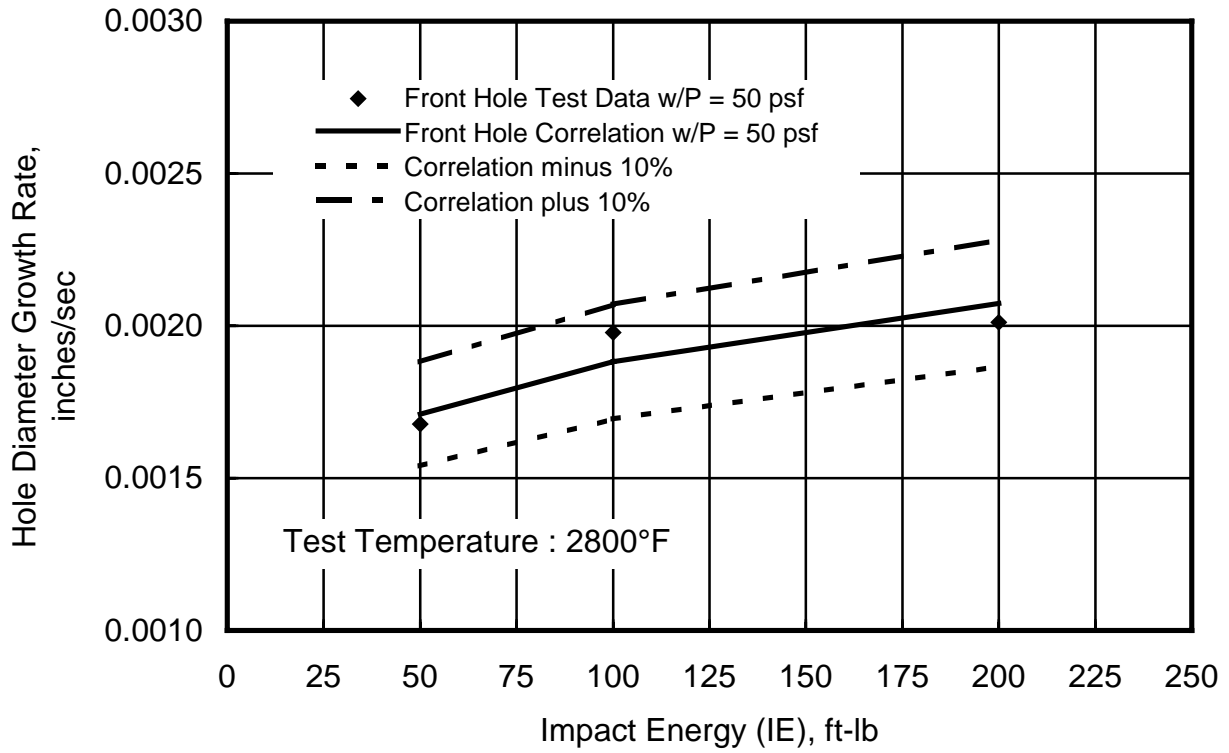With and Without An Impacted Hole

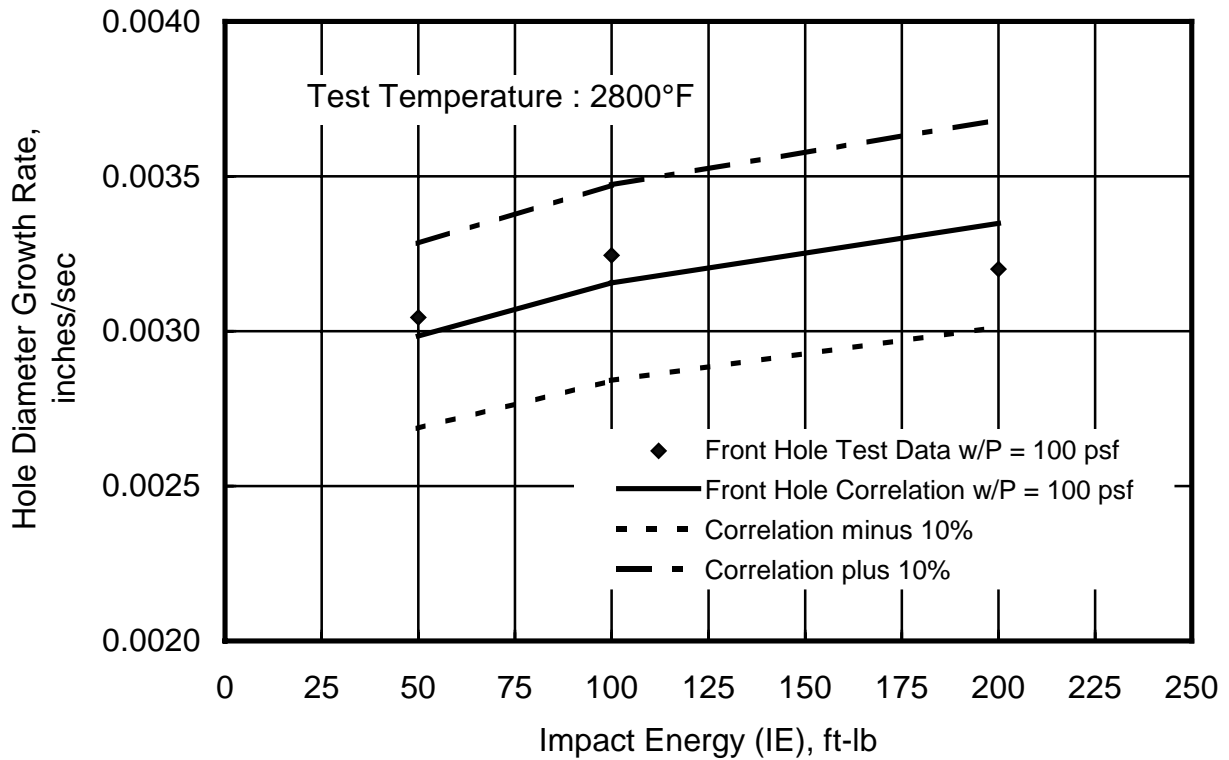Figure C-2 An Impacted RCC Front Hole Growth

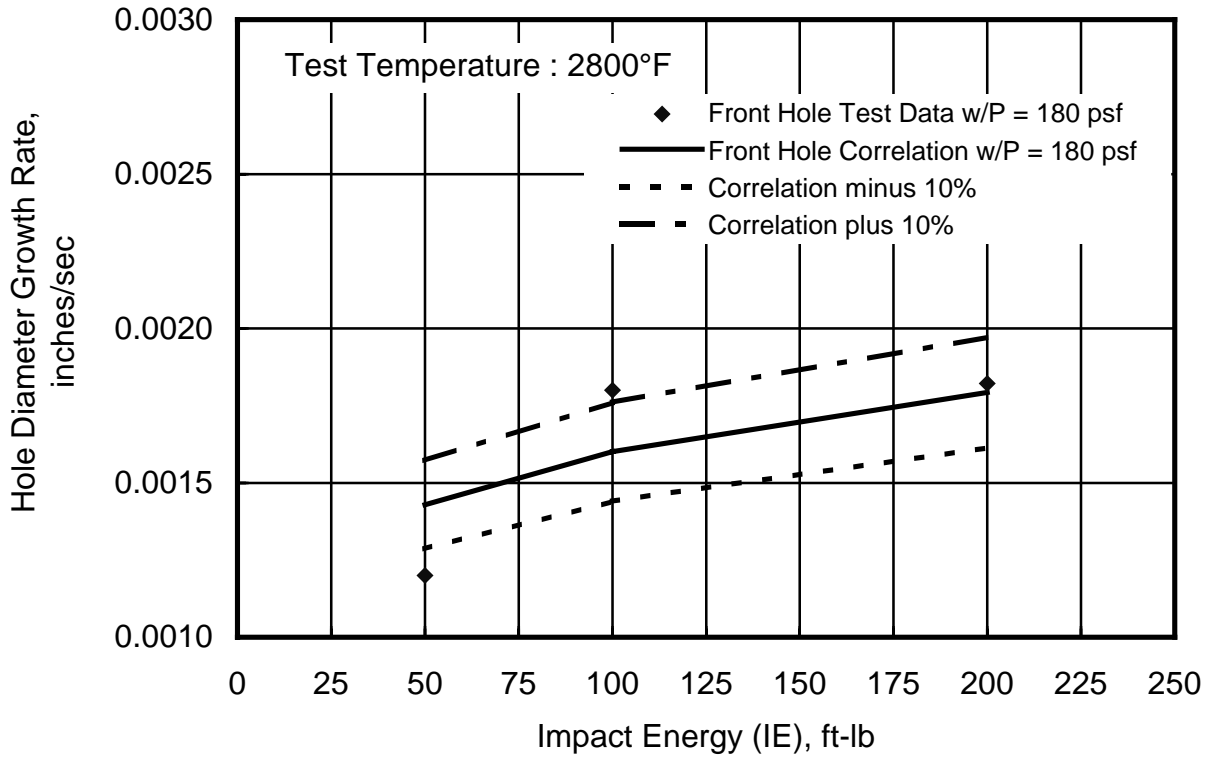Figure C-3 An Impacted RCC Front Hole Growth
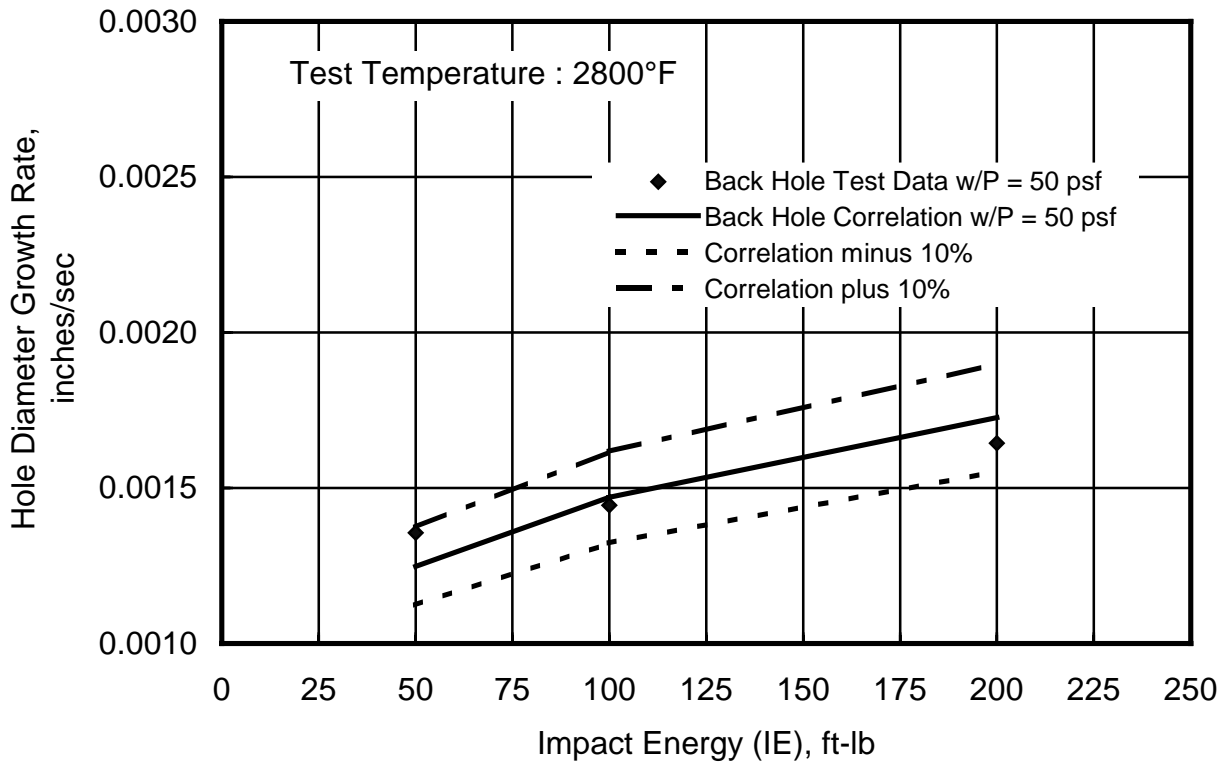
Figure C-4 An Impacted RCC Front Hole Growth

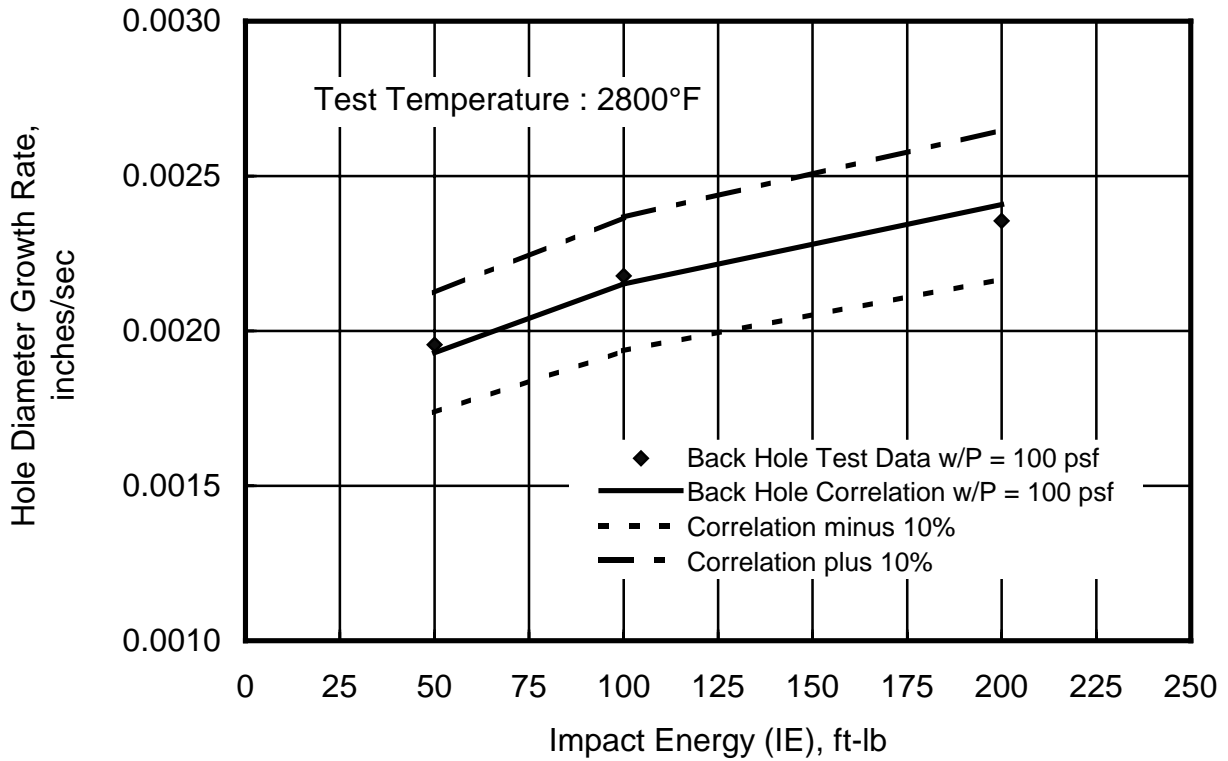Figure C-5 An Impacted RCC Back Hole Growth

Figure C-6 An Impacted RCC Back Hole Growth

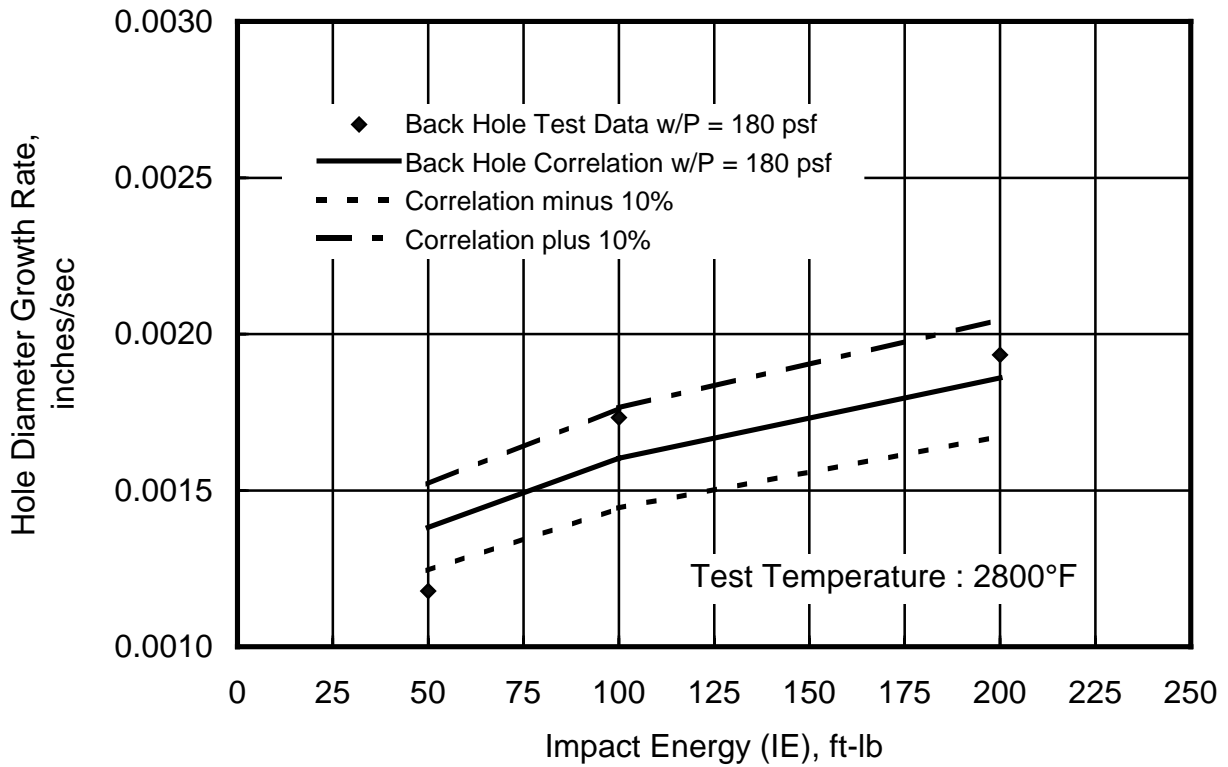Figure C-7 An Impacted RCC Back Hole Growth

COMPARISON OF
STEADY-STATE READINGS
BETWEEN LASER PYRO
AND
THERMOCOUPLES ON RCC CALIBRATION MODELS

The tables below were copied directly from a page in the Test Director's logbook and show differences in the laser pyro and thermocouple readings that have been typical for all RCC tests performed in this facility. TC1 is a surface thermocouple that was located in the center of the calibration puck; TC3 is another surface thermocouple that was located about halfway to the edge of the puck. Run 2-1726-7 used calibration model 2B24 that was used on a number of previous test programs, and run 2-1728-7 used a new RCC calibration model that ran a slightly higher temperature. The response from TC3 during run 1728 was about 350°F low because the TC was pulled back.

Run 2-1726-7:   10/27/97
Dual calibration model (pressure and heating rate) on left arm. Old RCC model 2B24 on right arm with centered and off-centered T/Cs (#1 and #3).

m (lb/s)	I (A)	p (psf)	Q (BTU/ft^{2}sec)	h-bulk BTU/lb	t/c 1 (°F)	t/c 3 (°F)	pyro (°F)
0.4	460	196	109	3195	2875	2850	2875
0.6	570	285	141	3084	3140	3100	3135
0.6	600	289	149	3199	3175	3150	3190
0.6	660	300	160	3441	3260	3220	3275

Run 2-1728-7:   10/29/97
Dual calibration model (pressure and heating rate) on left arm. New RCC model 1010 on right arm, with centered and off-centered T/Cs (#1 and #3).

m (lb/s)	I (A)	p (psf)	Q (BTU/ft^{2}sec)	t/c 1 (°F)	t/c 3 (°F)	pyro (°F)
0.4	460	196	109	2944	2580	2910

56

REPORT DOCUMENTATION PAGE

Form Approved
OMB No. 0704-0188

1. AGENCY USE ONLY *(Leave Blank)*	2. REPORT DATE March 2000	3. REPORT TYPE AND DATES COVERED NASA Technical Paper

4. TITLE AND SUBTITLE
Oxidation of Reinforced Carbon-Carbon Subjected to Hypervelocity Impact

5. FUNDING NUMBERS

6. AUTHOR(S)
Donald M. Curry, Vuong T. Pham, Ignacio Norman*, Dennis C. Chao*

7. PERFORMING ORGANIZATION NAME(S) AND ADDRESS(ES)

Lyndon B. Johnson Space Center
Houston, Texas 77058

8. PERFORMING ORGANIZATION REPORT NUMBERS
S-852

9. SPONSORING/MONITORING AGENCY NAME(S) AND ADDRESS(ES)

National Aeronautics and Space Administration
Washington, DC 20546-0001

10. SPONSORING/MONITORING AGENCY REPORT NUMBER
TP-2000-209760

11. SUPPLEMENTARY NOTES
* Boeing North American, Inc., Houston, Texas 77058

12a. DISTRIBUTION/AVAILABILITY STATEMENT

Available from the NASA Center for AeroSpace Information (CASI)
7121 Standard
Hanover, MD 21076-1320   Subject Category: 27

12b. DISTRIBUTION CODE

13. ABSTRACT *(Maximum 200 words)*
This paper presents results from arc jet tests conducted at the NASA Johnson Space Center on reinforced carbon-carbon (RCC) samples subjected to hypervelocity impact. The RCC test specimens are representative of RCC components used on the Space Shuttle Orbiter. The arc jet testing established the oxidation characteristics of RCC when hypervelocity projectiles, simulating meteoroid/orbital debris, impact the RCC material. In addition to developing correlations for use in trajectory simulations, we discuss analytical modeling of the increased material oxidation in the impacted area using measured hole growth data. Entry flight simulations are useful in assessing the increased Space Shuttle RCC component degradation as a result of impact damage and the hot gas flow through an enlarging hole into the wing leading-edge cavity.

14. SUBJECT TERMS

arc jet engines; arc discharges; impact damage; hypervelocity impact; impact prediction; computerized simulation; impact tests; debris; space debris; oxidation

15. NUMBER OF PAGES
63

16. PRICE CODE

17. SECURITY CLASSIFICATION OF REPORT	18. SECURITY CLASSIFICATION OF THIS PAGE	19. SECURITY CLASSIFICATION OF ABSTRACT	20. LIMITATION OF ABSTRACT
Unclassified	Unclassified	Unclassified	Unlimited

Standard Form 298 (Rev Feb 89) (MS Word Mar 97)   NSN 7540-01-280-5500
Prescribed by ANSI Std. 239-18
298-102

GENERAL INSTRUCTIONS FOR COMPLETING SF 298

The Report Documentation Page (RDP) is used in announcing and cataloging reports. It is important this information be consistent with the rest of the report, particularly the cover and title page. Instructions for filling in each block of the form follow. It is important to **stay within the lines** to meet **optical scanning requirements.**

Block 1. Agency Use Only (Leave Blank).

Block 2. Report Date. Full publication date including day, month, and year, if available (e.g. 1 Jan 88). Must cite at least the year.

Block 3. Type of Report and Dates Covered. State whether report is interim, final, etc. If applicable, enter inclusive report dates (e.g. 10 Jun 87 - 30 Jun 88).

Block 4. Title and Subtitle. A title is taken from the part of the report that provides the most meaningful and complete information. When a report is prepared in more than one volume, repeat the primary title, add volume number, and include subtitle for the specific volume. On classified documents enter the title classification in parentheses.

Block 5. Funding Numbers. To include contract and grant numbers; may include program element number(s), project number(s), task number(s), and work unit number(s). Use the following labels:

C	- Contract	**PR**	-	Project
G	- Grant	**TA**	-	Task
PE	- Program Element	**WU**	-	Work Unit Accession No.

Block 6. Author(s). Name(s) of person(s) responsible for writing the report, performing the research, or credited with the content of the report. If editor or complier, this should follow the name(s).

Block 7. Performing Organization Name(s) and Address(es). Self-explanatory.

Block 8. Performing Organization Report Number. Enter the unique alphanumeric report number(s) assigned by the organization performing the report.

Block 9. Sponsoring/Monitoring Agency Name(s) and Address(es). Self-explanatory.

Block 10. Sponsoring/Monitoring Agency Report Number. *(If known)*

Block 11. Supplementary Notes. Enter information not including elsewhere such as: Prepared in cooperation with...; Trans. Of ...; To be published in... When a report is revised, include a statement whether the new report supersedes or supplements the older report.

Block 12a. Distribution/Availability Statement. Denotes public availability or limitations. Cite any availability to the public. Enter additional limitations or special markings in all capitals (e.g. NOFORN, REL, ITAR).

DOD	-	See DoDD 5230.24, "Distribution Statements on Technical Documents."
DOE	-	See authorities.
NASA	-	See Handbook NHB 2200.2.
NTIS	-	Leave blank.

Block 12b. Distribution Code.

DOD	-	Leave blank.
DOE	-	Enter DOE distribution categories from the Standard Distribution for Unclassified Scientific and Technical Reports.
NASA	-	Leave blank.
NTIS	-	Leave blank.

Block 13. Abstract. Include a brief *(Maximum 200 words)* factual summary of the most significant information contained in the report.

Block 14. Subject Terms. Keywords or phrases identifying major subjects in the report.

Block 15. Number of Pages. Enter the total number of pages.

Block 16. Price Code. Enter appropriate price code *(NTIS only).*

Block 17. - 19. Security Classifications. Self-explanatory. Enter U.S. Security Classication in accordance with U.S. Security Regulations (i.e., UNCLASSIFIED). If form contains classified information, stamp classification on the top and bottom of the page.

Block 20. Limitation of Abstract. This block must be completed to assign a limitation to the abstract. Enter either UL (unlimited) or SAR (same as report). An entry in this block is necessary if the abstract is to be limited. If blank, the abstract is assumed to be unlimited.